An Experimental Investigation into the Passive Reconfiguration of Flexible Plates Near a Free Surface

Nicholas A. Scianna

Thesis submitted to the Faculty of the
Virginia Polytechnic Institute and State University
in partial fulfillment of the requirements for the degree of

Master of Science
in
Ocean Engineering

Christine Gilbert, Chair
Michael Philen
Olivier Courtier-Delgosha

April 25, 2022
Blacksburg, Virginia

Keywords: Reconfiguration, Flexible Plates, Fluid-Structure Interaction, Particle Image Velocimetry, Image Processing

An Experimental Investigation into the Passive Reconfiguration of Flexible Plates Near a Free Surface

Nicholas A. Scianna

ABSTRACT

Reconfiguration refers to the ability of a flexible structure to change its shape, allowing it to reduce its area perpendicular to the flow, to reduce drag. Decreasing the flexural rigidity of human-made structures can lead to improved designs that operate at higher propulsive efficiencies. The work presented in this thesis examines the physics surrounding a flexible plate under prescribed oscillatory heaving motions. White light movies were recorded at constant frequency and varying proximity to the free surface to investigate the change in reconfiguration as the plate approaches the free surface. Results, analyzed in terms of deformed plate shape, deflection, and plate tip kinematics, found that free surface effects increase the deflection of the plate as the plate approaches the free surface. Expanding on the initial experiments, a variety of frequencies were tested. The results show that each heaving frequency has a different critical height to the free surface in which deep water behavior is distinguished from shallow water behavior. At the critical depth, the plate deflection becomes asymmetric due to free surface effects. The second stage of experiments focused on measuring the fluid loading and fluid flow surrounding the flexible plate. The fluid loading, or drag force, acting on the plate was estimated by using a strain gauge load cell. Results of these experiments found that the drag force is equivalent on plates with lower heaving frequencies when compared to the highest heaving frequency tested due to increased reconfiguration at the higher frequency. The fluid moved from the keel to the edge of the plate as seen in the particle image velocimetry experiments. Higher heaving frequencies

created faster fluid flow off the plate and stronger tip vortices being shed from the plate. When the flexible plate operated at large distances from the free surface, the fluid dynamics showed the same behavior for the upstroke and downstroke of the plate. Whereas, when the plate operated close to the free surface, a vortex only forms on the upstroke, leading to asymmetric loading and deformations.

An Experimental Investigation into the Passive Reconfiguration of Flexible Plates Near a Free Surface

Nicholas A. Scianna

GENERAL AUDIENCE ABSTRACT

The ability for a structure to bend under loading and return to its original shape after the load is removed presents a desirable characteristic for structural design. The flexibility of the structure can lead to significant weight loss in contrast to rigid structures. In nature, almost all structures are able to bend when faced with fluid forces which decreases the loading the structure has to handle. Decreasing the stiffness of human-made structures can lead to improved designs that operate at higher propulsive efficiencies. The work presented here examines the physics surrounding a flexible plate under prescribed oscillatory heaving motions, which are motions that are purely vertical. White light movies were recorded at constant frequency and varying proximity to the free surface to investigate the change in plate shape as the plate approaches the free surface. Results, analyzed in terms of deformed plate shape, deflection, and plate tip kinematics, found that free surface effects increase the deflection of the plate as the plate approaches the free surface. Expanding on the initial experiments, a variety of frequencies were tested. The results show that each heaving frequency has a different critical height to the free surface in which deep water behavior is distinguished from shallow water behavior. At the critical depth, the plate deflection becomes asymmetric due to free surface effects. The second stage of experiments focused on describing the fluid loading and fluid flow surrounding the flexible plate. The fluid loading, or drag force, acting on the plate was estimated by using a strain gauge load cell. Results of these experiments found that the drag force is equivalent on plates with lower

heaving frequencies when compared to the highest heaving frequency tested due to increased reconfiguration at the higher frequency. The fluid moved from the center of the plate to the edge of the plate as seen in the particle image velocimetry experiments, which track the movement of particles in the fluid. Higher heaving frequencies created faster fluid flow off the plate. When the flexible plate operated at large distances from the free surface, the fluid flow showed the same behavior for the upstroke and downstroke of the plate. Whereas, when the plate operates close to the free surface, the fluid flow behaves differently leading to asymmetric loading and deformations.

Dedication

Dedicated to my parents who have made numerous sacrifices to allow me the opportunity to take on this rewarding challenge. Thank you.

Acknowledgments

I would like to acknowledge and thank my family for their unconditional love and support. Without you all, I would not be where I am today and your support has been crucial every step of the way. Love y'all!

I would also like to thank my lab mates who allowed me to bounce ideas off of them and were always willing to lend a helping hand. A special thanks to Dr. Javad Javaherian, Mark Shepheard, and James Duval that could be found in the lab at all hours with me.

Thank you to my advisor Dr. Christine Gilbert for constantly encouraging me to excel as an experimentalist and student. Your advisement has constantly pushed me to dig deeper and challenge myself to take on new endeavors.

Finally I would like to acknowledge the support and funding from the National Science Foundation Grant 1944614.

Contents

List of Figures xi

List of Tables xiv

1 Introduction 1

1.1 Literature Review . . . 2

1.1.1 Physics of Reconfiguration . . . 2

1.1.2 Flexible Plate Reconfiguration . . . 4

1.1.3 Benefits of Biologically Inspired Structures . . . 5

1.2 Project Scope . . . 6

2 Experimental Setup 8

2.1 Experimental Setup . . . 8

2.1.1 Actuation System . . . 8

2.1.2 Test Specimen . . . 9

2.2 Instrumentation . . . 10

2.2.1 Potentiometer . . . 10

2.2.2 Strain Gauge Load Cell . . . 11

2.2.3 Data Acquisition System . . . 11

2.3 Image Processing 12
2.3.1 High Speed Camera 12
2.3.2 Gradient-Based Edge Detection 13
2.4 Particle Image Velocimetry 16
2.5 Experimental Matrix 18
2.5.1 Effect of Proximity to the Free Surface on Reconfiguration for a Flexible Plate Under Prescribed Constant Frequency Oscillatory Motion . 18
2.5.2 Effect of Varying Frequency of Prescribed Oscillatory Motion on the Passive Reconfiguration of a Flexible Plate 20
2.5.3 Fluid Loading on Heaving Flexible Plates 20
2.5.4 Fluid Flow Surrounding Heaving Flexible Plates 21
2.6 Uncertainty in Measurement Techniques 21

3 Results and Discussion **24**

3.1 Effect of Proximity to the Free Surface on Reconfiguration for a Flexible Plate Under Prescribed Constant Frequency Oscillatory Motion 24
3.1.1 Structural Response Dependence on Height to the Free Surface . . . 25
3.1.2 Symmetry in Plate Deflection 28
3.1.3 Plate Tip Deflection and Kinematics 30
3.2 Effect of Varying Frequency of Prescribed Oscillatory Motion on the Passive Reconfiguration of a Flexible Plate 33

3.2.1 Dimensional Results 34
3.2.2 Non-Dimensional Analysis 37
3.3 Fluid Loading on Heaving Flexible Plates 40
3.3.1 Plate Drag 41
3.4 Fluid Flow Surrounding Heaving Plates 46
3.4.1 Dynamic Masking 46
3.4.2 Velocity Field and Streamlines 48

4 Conclusions and Future Work **53**
4.1 Conclusions 53
4.2 Future Work 55

Bibliography **57**

Appendices **59**

Appendix A Prescribed Motion Repeatability **60**
A.1 Repeatability of the Prescribed Oscillatory Motion 60

List of Figures

2.1 Experimental setup diagrams depicting the a) front view from the perspective of the camera and b) the side view including the camera. 9

2.2 Flexible plate testing specimen with top view, front view, and dimensions. . 10

2.3 Strain gauge load cell attached to the heave post used to measure the drag force acting on the plate. 12

2.4 Laboratory image of the controlled heave experimental setup with high speed camera field of view highlighted. 13

2.5 The a) raw image of a white light movie and b) detected plate edge in red on the same raw image. 14

2.6 Conceptualization of the nearest neighbor search algorithm with red arrows representing the path of the search. 15

2.7 Snapshot of the calibration plate with the intersection points marked in red. 16

2.8 Experimental set up showing the laser sheet utilized for the PIV experiments. 17

2.9 Instantaneous flow velocity uncertainty at f = 0.50 Hz and h = 18.5 cm. . . 22

2.10 Instantaneous correlation value at f = 0.50 Hz and h = 18.5 cm. 23

3.1 Time history of keel location in reference to the undisturbed free surface at varying h values. 26

3.2 Deformed plate shapes at the maximum keel depth for all h values. 27

3.3 Deformed plate shapes at the minimum keel depth for all h values. 28

3.4 Schematic depicting the physical representation of positive deflection. 28

3.5 Deflection along the length of the plate at all h values plotted in the body-fixed reference frame. 29

3.6 Time history of the tip position corresponding to conditions closest and furthest from the undisturbed free surface. 31

3.7 Time history of the tip deflection corresponding to conditions closest and furthest from the undisturbed free surface. 32

3.8 Plate tip and keel velocity time histories for a h value of 5.3 cm. 33

3.9 Tip deflection at maximum keel depth for varying h values. 34

3.10 Keel heaving history with reference to the undisturbed free surface for prescribed heaving frequencies of a) 0.50 Hz, b) 0.44 Hz, c) 0.38 Hz, and d) 0.31 Hz. 36

3.11 Reconfigured plate shapes at the maximum keel height for frequencies of a) 0.50 Hz, b) 0.44 Hz, c) 0.38 Hz, and d) 0.31 Hz. 37

3.12 Dimensionless plate reconfiguration for frequencies of a) 0.50 Hz, b) 0.44 Hz, c) 0.38 Hz, and d) 0.31 Hz at maximum keel depth. 38

3.13 Dimensionless maximum deflection across various frequencies and submergence heights. 39

3.14 Dimensionless maximum deflection versus Strouhal number across frequencies and h values. 40

3.15 Unfiltered drag data for three trials with plate specimen and one trial without the plate specimen. 41

3.16 The (a) raw data (—) and filtered data (—) of the plate of one trial and (b) spectral analysis of the frequency domain. 42

3.17 A time history of plate drag (—) and keel position (—) for various heights to the free surface and frequencies. 44

3.18 Comparison of plate drag at h of 30.5 cm (—) and 6.0 cm (—) at heaving frequencies of a) 0.50 Hz and b) 0.31 Hz. 45

3.19 PIV data processing from the a)raw image to the b)masked image which result in the c)velocity vectors and d)streamlines. 47

3.20 Velocity field measurements with streamlines depicting the direction of fluid flow at f = 0.50 Hz and h = 18.5 cm. 49

3.21 Velocity field measurements with streamlines depicting the direction of fluid flow at f = 0.31 Hz and h = 18.5 cm. 50

3.22 Velocity field measurements with streamlines depicting the direction of fluid flow at f = 0.50 Hz and h = 6.0 cm. 51

3.23 Velocity field measurements with streamlines depicting the direction of fluid flow at f = 0.31 Hz and h = 6.0 cm. 52

A.1 Potentiometer time history agreement at one frequency and one height to the free surface. 60

List of Tables

2.1 Experimental matrix spanning all controlled oscillatory heaving experiments. 19

3.1 Constant Frequency Experiments Line Styles 26

3.2 Varied Frequency Experiments Line Styles 35

List of Abbreviations

ρ	Density
C_D	Coefficient of Drag
Ca	Cauchy Number
D	Drag Force
E	Flexural Rigidity
f	Heaving Frequency
K	Bulk Modulus of Elasticity
L	Amplitude of Oscillation
St	Strouhal Number
U	Free Stream Velocity
V	Vogel Exponent

Chapter 1

Introduction

Few structures in nature are truly rigid. From the flapping motion of manta ray fins to the compliant bending of seagrass in ocean currents, low flexural rigidity is a key characteristic in many naturally occurring structures. Seagrass under current loads exhibits passive reconfiguration, where the flexural rigidity of the plant does not change over time, and the seagrass bends to become streamlined in the flow. Manta rays are able to vary the stiffness of their fins as they cruise through the water column, actively reconfiguring them to a desired shape. Reconfigured shapes may be optimized for a variety of intentions, such as drag reduction or maximum power. Evolution has fine-tuned biological systems such that the cruising speed of many aquatic animals occurs at the optimal Strouhal number for maximum efficiency of thrust production. Current engineering practices consist of designs that prioritize stiffness and rigidity to withstand load requirements, but this narrows the design space. Decreasing the flexural rigidity of structures leaves vast room for improvement in system design. Deriving inspiration from nature, systems can be designed that weigh less, are more efficient, and have heightened longevity. The incentives of flexible structures have been widely acknowledged, but further experimental research is needed to define the fluid-structure interaction of flexible structures under fluid loading. Specifically, unsteady flows near a free surface present particularly difficult challenges, as free surface effects contribute to the reconfiguration of the flexible structure in more complex ways. Work in this field will benefit the expansion of the design space and lead to human-made structures operating at

heightened efficiencies in comparison to current designs.

1.1 Literature Review

1.1.1 Physics of Reconfiguration

In nature, forces acting on a moving body in a fluid medium are commonly derived from the fluid moving around it. The force opposite to the direction of travel within a fluid is drag. Human-made structures are optimized for drag with CFD models and experiments which attempt to streamline a rigid structure to best the hydrodynamics. Objects in nature leverage their low flexural rigidities to alter their shape to reduce drag. Vogel (1984) introduced this concept of deforming to reduce the load acting on a body which is referred to as reconfiguration [1].Reconfiguration and deformation are terms that may be used interchangeably since both refer to the change in the structural shape or length. Conceptualizing the physics of this phenomenon on a basic level, the body undergoing the fluid loading reconfigures its shape which will reduce the area perpendicular to the flow. This lessens the area that the fluid may act on, making the body more streamlined [2, 3]. Studies into reconfiguration have led to findings that suggest flexible bodies do not encounter the same drag effects as rigid bodies and thus drag is not proportional to the square of velocity. Instead, it is proportional to some factor dependent on the reconfiguration of the structure which has been denoted as the Vogel exponent (V)

$$F \propto U^{2+V},$$

where U is the freestream velocity and F is the drag force [1, 2]. The reduction in drag

of flexible bodies, or the need for the Vogel exponent, has been found by several other researchers including Alben *et al* (2002) and Gosselin *et al.* (2010). The concepts found in the literature have sparked sparse interest in the engineering field with flexible structures under constant fluid loads, mostly undergoing wind tunnel experiments. Vogel phrased it best when comparing natural structures to human-made structures saying, "... better bent than broken" [1].

The concept of reconfiguration first progressed into a theoretical model when Alben *et al.* (2002) coupled experiments with theoretical math models to investigate the drag reduction of a bending body. In this investigation, a gap in experimental studies of fluid-structure interactions pertaining to very flexible structures that reconfigure was acknowledged as the target research objective. The experiment consisted of a flexible fiber which was subject to flow in a soapy film. The soapy film was gravity fed through the testing section in which the flow rate could be controlled to vary the free stream velocity which forced the fiber to reconfigure. The experimental results were confirmed with numerical analysis of the solutions for the reconfigured fiber shapes. This work set the basis in which observations of reconfiguration made in nature may be applied to engineering principles. A two-dimensional potential flow model was used to calculate the drag acting on the body. Alben *et al.* (2002) defined a non-dimensional drag force,

$$D = C_D \eta^2 \text{ , where } \eta = \sqrt{\frac{\rho f L^2 U^2/2}{E/L}}.$$

Here, ρ is the density of the fluid, f is the fluid thickness, L is the length of the specimen, and E is the rigidity. The term η, which is a drag scaling factor that accounts for material properties, was chosen such that it scales with drag in the same way velocity does. For rigid structures, drag scales with the square of velocity as well as . This scaling scheme was tested in experiments with a rigid fiber to validate the relationship between and free stream

velocity. Conclusions of this work found that the drag of the flexible fiber scaled with $\eta^{4/3}$, reiterating the conclusion set forth by Vogel (1996). An asymptotic trend was also found in the deformed fiber shapes as the free stream velocity increased based on similar length scales. Limitations of this work apply to the testing specimen, where only one material was tested. The scaling of drag only applies to the specific tests that were presented and no prediction models for deformation or loading were presented [4, 5].

1.1.2 Flexible Plate Reconfiguration

Gosselin *et al.* (2010) expanded on the groundwork of Alben by continuing experimental investigation of two-dimensional reconfiguration of flexible structures. A systematic approach was taken to investigate the passive reconfiguration of flexible rectangular and cut disk plates. This study included a deep investigation into the proper non-dimensional scaling of the problem and theoretical prediction of deformations by modeling the flexible plate as a beam. Gosselin *et al.* (2010) completed wind tunnel experiments on a wide range of flexible plates which were allowed to reconfigure around a rod placed at the center of the plate. The fluid loading on the plate remained constant and was measured by a load cell connected to the model. The experimental results showed that the Vogel exponent derived from the fiber experiments matched that which was calculated for the flat rectangular plates. This Vogel exponent did not match for the cases where the cut disk geometries were tested. Similarly to Alben *et al.* (2002), an asymptotic trend in the reconfigured shape of the plate was observed for both small and large Cauchy numbers,

$$Ca = \frac{\rho U^2}{K},$$

which is dependent on the flow velocity (U), fluid density (ρ), and bulk modulus of elasticity (K) [6].

The results of the wind tunnel experiments were then analyzed non-dimensionally resulting in four characteristic values which can describe the reconfiguration under steady flow. The four dimensionless numbers are the Cauchy number, reconfiguration number, aspect ratio, and blockage coefficient. The reconfiguration number is first proposed here to describe the reconfiguration of a flexible structure as a function of the Cauchy number and drag coefficient. The ability to analyze the problem with dimensionless parameters enabled the authors to develop a theoretical model which predicted the deflected plate shape. The plate was modeled as a two-dimensional beam problem under an adjusted drag load according to the reconfiguration number stated previously. These predictions are strictly limited to plates which are subject to constant loading where the drag force is not changing with respect to time over the course of the study [6].

1.1.3 Benefits of Biologically Inspired Structures

Biological swimmers have been found to operate at high efficiencies in comparison to human-made robotic swimmers which is dependent on many factors that Nesteruk (2014) proved to include body shape, advance velocity, and swimming mode [7]. The efficiency of biological swimmers has led to a lot of recent work in the biological systems engineering field which investigates the possible advantages of flapping swimmers. Such swimmers may be models utilizing airfoils with both heaving and pitching motions. Floryan (2017) completed water tunnel experiments on rigid airfoil shapes which are subject to both pitching and oscillatory heaving motions and found that thrust and drag are dependent upon both Strouhal number and frequency of oscillation [8]. This shows that the high efficiency range for Strouhal number,

$$St = \frac{fL}{U},$$

in airfoils coincides with that of biological systems which are tuned for peak thrust efficiency. Dependency on Reynolds number has also been found to impact the peak efficiency Strouhal number at low Reynolds which moves the peak efficiency point for swimmers [9, 10, 11].

Replicating the high efficiency of manta rays, which has been found to be upward of 89% by Fish (2016), requires analysis of flexible structure to understand the physics of the flapping behavior [12]. Alben (2008) first investigated a similar problem by analyzing an elastic sheet which produces a vortex sheet wake. The efficiency was found to increase with decrease in flexibility of the elastic sheet and reach a maximum value when pitching frequency was 0.27 [13]. Floryan (2020) furthered the work on flexibility finding optimal distribution of flexibility would be one that creates a stiff leading edge and a more flexible trailing edge [14]. Simplistic manta ray robots have been manufactured in the laboratory setting to apply the knowledge of reconfiguration to human-made materials. The models created by Wang *et al.* (2009), Chen *et al.* (2012), and Moored *et al.* (2011) utilized flexible structures for the wings, actuated by smart materials with a rigid body in between [15, 16, 17]. The models have not been able to reach the same efficiency level of what is observed in nature and are only optimized for the manufactured model rather than optimizing the structure by understanding the fluid-structure interaction. Although these models lack the same thrust efficiency, they set a strong groundwork in which engineered materials may be used to achieve a desired reconfigured plate shape to produce thrust.

1.2 Project Scope

Current literature draws attention to biological systems for inspiration and presents a strong understanding of reconfiguration under constant flow field conditions. Work has also been completed in understanding rigid airfoil structures which heave and pitch in a similar fashion

to fish. ***A gap in understanding the physics of flexible plate reconfiguration near a free surface*** has been identified which will enable the development of more efficient system designs moving forward. This thesis will present experimental results pertaining to the passive reconfiguration of flexible plates near a free surface through a systematic approach of varying parameters. From videos taken with high speed cameras, gradient based edge detection techniques yield the deflection and reconfigured plate shapes. A better understanding of the fluid flow around the plate with prescribed oscillatory heaving motion is shown through particle image velocimetry (PIV) measurements. The scope of this paper is limited to one plate model and the future of this work will be discussed in detail.

Chapter 2

Experimental Setup

The experimental setup, instrumentation, post-processing techniques, and experimental matrix will be discussed in this chapter. The two types of post-processing methods that will be discussed include digital image processing and particle image velocimetry.

2.1 Experimental Setup

The experiments conducted in the Virginia Tech Hydroelasticity Laboratory took place in a nearly cubic water tank that is 4 feet wide, 4 feet long, and 3 feet tall. Black window tint lines the back wall of the tank creating a dark background for the camera view. The water level was held constant at 66 centimeters for all experiments that will be discussed.

2.1.1 Actuation System

An oscillatory heaving motion is prescribed to the plate by a 24-V stepper motor (Nema 23) and motor controller. The rotational motion from the motor is translated to pure heave motion by connecting a coupler on the motor output shaft to linear bearings which slide on the t-slot framing that encases the tank. The experimental setup diagram is depicted in Fig. 2.1 from the 2.1a front and 2.1b side, where all components may be seen. The amplitude of the prescribed heaving motion is 5.1 centimeters based on the size of the shaft coupler

attachment.

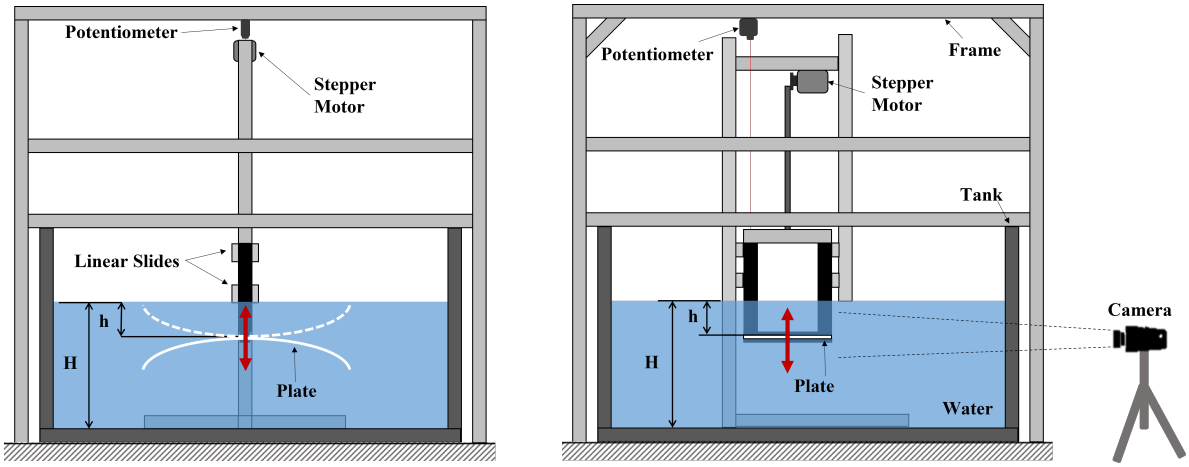

(a) Front View (b) Side View

Figure 2.1: Experimental setup diagrams depicting the a) front view from the perspective of the camera and b) the side view including the camera.

2.1.2 Test Specimen

A single geometry was selected for initial experiments. The flexible plate is a 1.6 mm thick ultra high molecular weight (UHMW) polyethylene plate with dimensions 30.48 cm in width and 60.96 cm in length. The density of the plate is approximately 941 kg/m^3 with a flexural modulus between 552 MPa and 758 MPa. An aluminum keel divides the plate into two even unsupported sections. The metal keel consists of two bar stock pieces that are 30.48 cm long, 2.54 cm wide, and 6.35 mm thick. The two metal keel bars clamp together around the UHMW plate and are secured to the t-slot framing rig which oscillates in the water column. The keel separates the plate into two plates with unsupported lengths of 29.21 cm on each side. The camera focuses on only one half of the plate since both sides behave symmetrically. The dimensions discussed are shown in Fig. 2.2 where the front view corresponds to the view of the camera during experiments.

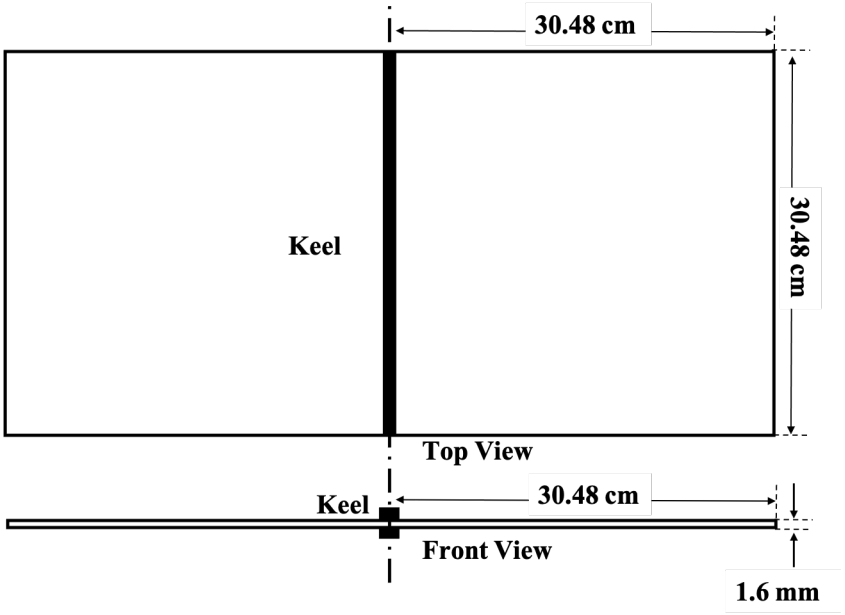

Figure 2.2: Flexible plate testing specimen with top view, front view, and dimensions.

2.2 Instrumentation

The measurement equipment used in this experiment are described in the subsections that follow. These include a string potentiometer, load cell, high-speed cameras, and PIV system.

2.2.1 Potentiometer

The heave motion time history is recorded with a string potentiometer which is suspended on the rig as seen in Fig. 2.1. The SGD-80-3 resistive linear position string potentiometer sampling at 2000 Hz is positioned perpendicular to the keel such that the measured movement is purely heave. Calibration of the potentiometer is set to be zero when the plate is at the free surface such that the data read depicts the instantaneous distance to the undisturbed free surface. H denotes the water level in the tank from the bottom of the tank to the undisturbed free surface, while h represents the keel height to the free surface.

2.2.2 Strain Gauge Load Cell

A PCB Load and Torque strain gauge load cell was utilized to measure the fluid loads acting on the system. The load cell is embedded into the midpoint of the metal heave post as seen in Fig. 2.3. Data was sampled at 2000 Hz and synchronized with the camera system by recording the voltage of the trigger signal. The data was then shifted in post-processing such that all instrumentation data was synchronized with the recorded images. The author acknowledges that the movement of the heave post is not purely vertical. At its largest pulling angle, the vertical component which acts solely in the direction of travel for the plate is 99.8% of the total force which is read by the load cell. Since the heave post connects the linear slides to the coupler on the DC motor, the resultant force acts at an angle rather than purely in heave. The heave post, with the load cell attached, is 39.5 cm long, and the length of the coupler from its center to the attachment post is 2.54 cm. The maximum angle that the heave post reaches occurs when the length between the center of the coupler and the attachment point is perpendicular to the motion of the plate. In the future experiments, the linear actuators will be used to ensure the load measured is acting solely in the heaving direction.

2.2.3 Data Acquisition System

The potentiometer connects to an NI PXIe-1082 DAQ through a PXIe-8821 controller module. The DAQ is fitted with NI PXIe-4492 analog input and NI TB-4330 8 Ch bridge input modules that interface with each instrument as well as the pulse generator. The experiments utilize a Berkley Nucleonics 577 Digital Delay pulse generator to provide the digital signal to the DAQ system as well as the camera to initiate data collection. This enables the data to be taken simultaneously to ensure that an accurate representation of the experiment is

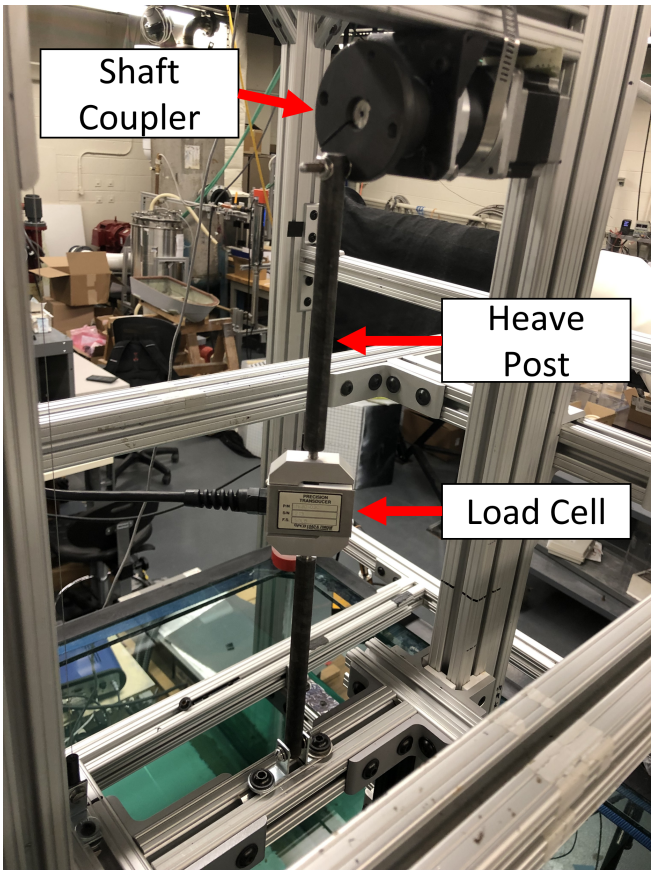

Figure 2.3: Strain gauge load cell attached to the heave post used to measure the drag force acting on the plate.

seen when comparing data of the same time step. Synchronization between instruments was essential to synchronize the data across runs during post-processing of the experiments.

2.3 Image Processing

2.3.1 High Speed Camera

A single Phantom VEO 710 S high speed camera was utilized to capture deformation of the flexible plate along its length. The high speed camera has a maximum frame rate of over

7,000 fps at one megapixel resolution. The field of view for the high speed camera captures the plate from the keel, where no deflection exists due to the clamped boundary condition, to the unsupported edge of the plate which may be seen in Fig. 2.4. Videos were recorded at 400 frames per second which was determined to provide the desired fidelity in the initial experiments.

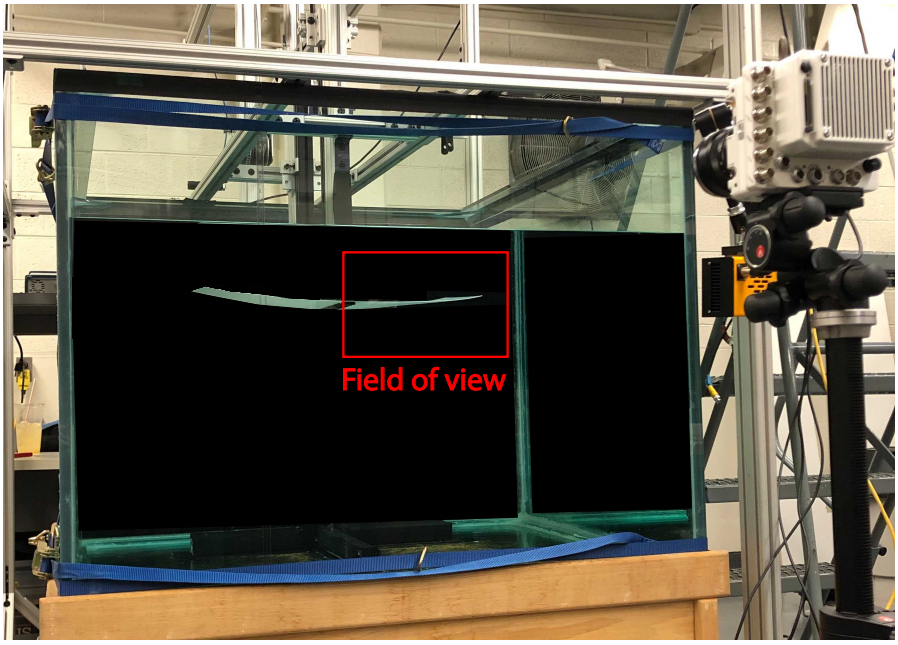

Figure 2.4: Laboratory image of the controlled heave experimental setup with high speed camera field of view highlighted.

2.3.2 Gradient-Based Edge Detection

A high contrast testing environment is established by utilizing a bright white testing specimen with a dark background. This is seen in Fig. 2.5a which shows a representative image from a trial without any filtering applied. Image post processing has been completed utilizing a gradient-based edge detection technique to find and trace the bottom edge of the plate specimen. The Sobel method was utilized for edge detection which defines all edges within

the image. A nearest neighbor proximity search algorithm was implemented utilizing the

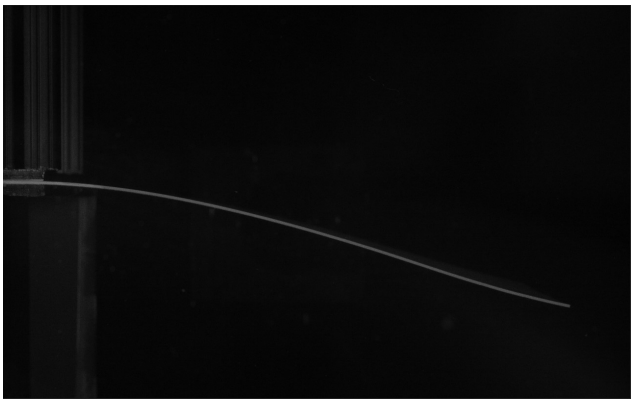

(a) Raw Image

(b) Raw Image with Detected Edge

Figure 2.5: The a) raw image of a white light movie and b) detected plate edge in red on the same raw image.

results of the Sobel operation to find and record the pixel coordinates of the desired edge. Fig. 2.5b shows the original image with the reconfigured plate edge shown in red on top of the image for reference. The nearest neighbor algorithm functions by first prioritizing the pixel immediately to the right of the current pixel coordinate. If the pixel does not belong to the edge and is detected as a black pixel, the algorithm then moves a set number of pixels down and begins to search for a white pixel moving upwards. The set number of pixels used in the search for a white pixel was varied based on a case-to-case basis to best fit the parameters of the run. Since the plate is continuous, a white pixel should be detected in every

column. However, foreign particles present in the testing facility cause errors in the tracing algorithm. Some particles may block the plate and create a gap in the detected edge. In this case, the algorithm completes a column sweep and moves to the next column to continue searching for white pixels. A conceptualization of the search algorithm may be seen in Fig. 2.6 with the red arrow representing the path of the algorithm. Other foreign particles as

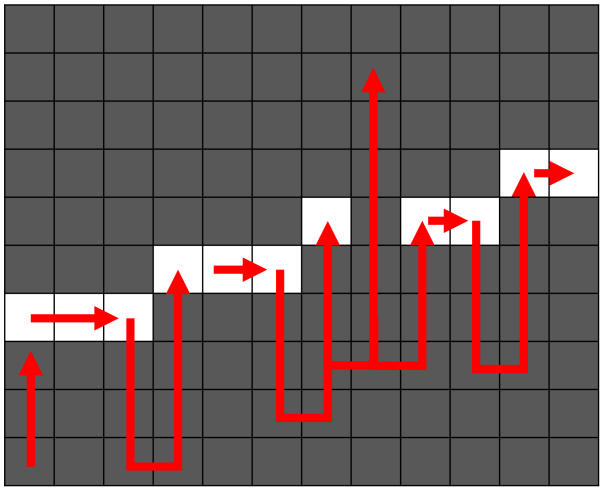

Figure 2.6: Conceptualization of the nearest neighbor search algorithm with red arrows representing the path of the search.

well as bubbles reflect the LED lights and appear white on the black background, creating a strong gradient. To mitigate discrepancies in the detected edge, a polynomial fit of the traced coordinates was completed. The coordinates of the detected edge are recorded and saved for further analysis and comparison. The pixel coordinates are used in conjunction with a calibration factor to transition to a distance coordinate system. A calibration plate was utilized to determine the calibration factor shown in Fig. 2.7. The red markers correspond to the selected intersection points on the plate from the calibration. The pixel coordinates in both the X and Y directions are plotted against the known distance coordinates to develop a mapping equation. The equations generated are linear scaling factors which is confirmed by the root means square fits of the data to the trendlines. The linear fit also shows that no fish-eye effects are occurring in the camera throughout the testing section.

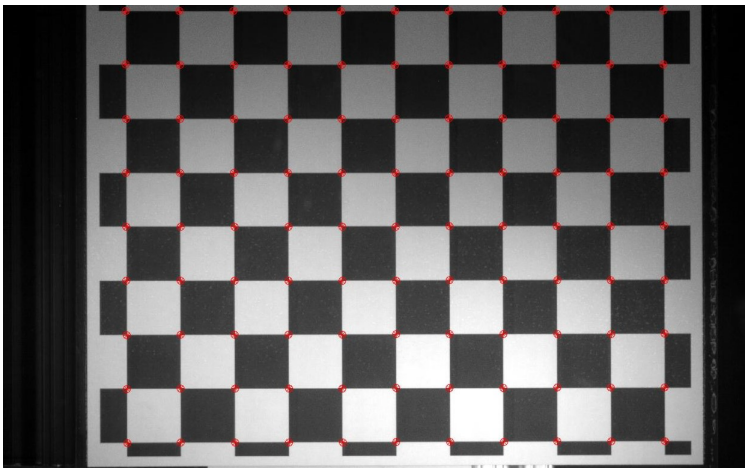

Figure 2.7: Snapshot of the calibration plate with the intersection points marked in red.

2.4 Particle Image Velocimetry

Planar particle Image Velocimetry (PIV) is an experimental technique that allows for flow visualization on a 2-D plane. In order to visualize the flow, the water is seeded with LaVision 20 μm polyamide particles. These are illuminated with dual laser heads which pulse at a set frequency in synchronization with a high speed camera. Within each 32 x 32 pixel interrogation window, 2-D cross correlation was performed to calculate the most probable path that each illuminated particle has traveled over the change in time. All interrogation windows had 50% overlap for cross correlation. Each interrogation window yields a single velocity vector as a result of the analysis. The velocity field may then be used to calculate other characteristics of the full-field flow such as pressure, streamlines, and vorticity.

The PIV experiments conducted to evaluate the flow around the flexible plate were completed in the same facility utilizing the plate specimen seen in Fig. 2.2. A rectangular section was cut from the wood base supporting the underside of the tank such that the laser light sheet could be illuminated from the bottom of the tank toward the free surface. The laser sheet could not be projected from the side of the tank due to the high deflection angles that were

seen in the earlier experiments. The plate tip-deflection would have blocked the laser from illuminating the particles behind it. The laser sheet may be seen in Fig. 2.8, creating a two-dimensional plane at the center of the flexible plate to perform PIV measurements.

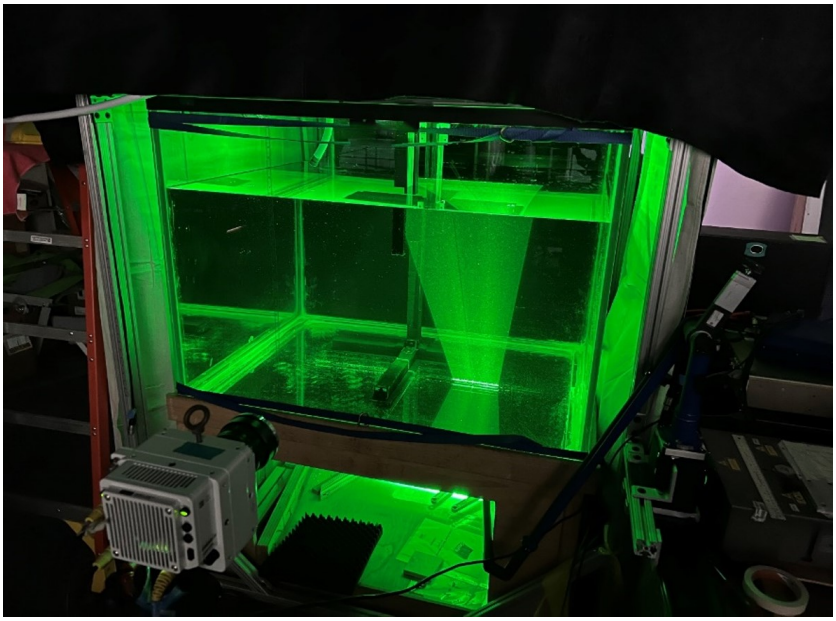

Figure 2.8: Experimental set up showing the laser sheet utilized for the PIV experiments.

A Photonics Industries DM30-527 dual head laser system provides laser beams with a maximum pulse energy of 60 mJ at 1 kHz. The two beams are reflected by a 90 degree mirror into a LaVision laser guiding arm which gives a large amount of flexibility to where the laser may be placed. The laser guiding arm extends underneath the tank and terminates into a LaVision collimator with a -20 mm focal length lens. Multiple lenses were tested to determine which lens gave the best illumination throughout the entire water column, while still giving the desired width of the laser sheet needed to capture the entire testing section. The laser light sheet was aligned at the center of the plate to minimize the 3-D effects within the flow field measured.

2.5 Experimental Matrix

Four separate experiments were conducted throughout the course of this investigation. Those four experiments are prescribed heaving motions of constant frequency, prescribed heaving motions of varied frequency, varied frequency with load cell analysis, and particle image velocimetry. The experimental matrix seen in Table 2.1 consolidates each of the four experimental matrices into one overarching matrix. In these experiments, the deformation (or reconfiguration) was measured using white light movies. A load cell was used to measure the total force on the plate under its prescribed motion. PIV measurements were taken to quantify the flow around the plate. The results of these measurements will be discussed with regard to the average depth of the plate below the free surface, h, and the frequency of oscillation.

White light movies were taken with a high–speed camera and LED lights. Quantitative measurements of deflection were obtained using a gradient-based edge detection technique discussed in Sec. 2.3.2.

Specific h values as well as frequencies were selected to conduct PIV experiments due to limitations in equipment availability. The selected values were minimums and maximums of each respective category to span the plausible values given the current experimental setup.

2.5.1 Effect of Proximity to the Free Surface on Reconfiguration for a Flexible Plate Under Prescribed Constant Frequency Oscillatory Motion

The first set of experiments were designed to analyze the effect of free surface proximity on plate reconfiguration. The average height to the free surface, h, was systematically adjusted

Table 2.1: Experimental matrix spanning all controlled oscillatory heaving experiments.

Depth (cm)	Heaving Frequency (Hz)				Method		
h	0.50	0.44	0.38	0.31	White Light	PIV	Load Cell
5.3	✓				✓		
6.0	✓	✓	✓	✓	✓	✓	✓
8.0	✓				✓		
9.0	✓	✓	✓	✓	✓		
10.6	✓				✓		
12.0	✓	✓	✓	✓	✓		
15.0	✓	✓	✓	✓	✓		
15.5	✓				✓		
18.5	✓	✓	✓	✓	✓	✓	
20.5	✓				✓		
25.5	✓				✓		
30.5	✓	✓	✓	✓	✓		✓

with increased fidelity towards the free surface to best define the free surface effect and the relationship between plate deflection and proximity to the free surface. The heaving frequency input was kept constant at 0.5 Hz for all trials with the only variation being the average height to the free surface. At each h value, three trials were completed to ensure repeatable results were gathered for each trial.

The stepper motor was started prior to data sampling and allowed to run such that the plate reached a steady state in terms of deflection during the oscillatory heave motion prescribed. A steady state was determined to be reached after a set amount of time had elapsed after initiating the motor motion, which was confirmed in the post processing of the data. Once the motor and plate were up to speed, the pulse generator triggered data acquisition and data was taken for both the camera and potentiometer simultaneously. Five seconds of data was recorded and saved such that two complete oscillations were captured. This allowed the beginning of any trial to be initiated at any instantaneous time rather than requiring a trigger for the motor which would require the phase of the motor to be monitored. The

data has been adjusted in the post process stage such that all data began at the closest keel location to the free surface.

2.5.2 Effect of Varying Frequency of Prescribed Oscillatory Motion on the Passive Reconfiguration of a Flexible Plate

The second set of experiments were conducted with the same procedures as the constant frequency experiments. Additional heaving frequencies were added to further investigate the role of frequency on plate reconfiguration. Frequencies of 0.5, 0.44, 0.38, and 0.31 Hz were tested by varying the frequency of the function generator from 2000 Hz to 1250 Hz in increments of 250 Hz. Heights to the free surface were also altered to have an increased focus on the region in which free surface effects were predominantly seen. This led to a large gap between the deepest heights and an increased amount of tests at the shallower h values.

2.5.3 Fluid Loading on Heaving Flexible Plates

Experiments were conducted including a load cell attached to the heave post to analyze the plate drag throughout a heaving oscillation. Experiments were conducted at average heights to the free surface of 6.0 cm and 30.5 cm, spanning the range of heights tested for the varied frequency experiments. The maximum and minimum frequencies tested in the varied frequencies were also utilized within the load cell experiments. White light movies were recorded to compare the results of the plate deflection in the load cell experiments to the results of the varied frequency experiments to confirm the repeatability of the setup and plate deformations. The data was synchronized in the post-processing by recording the voltage of the trigger signal to find the exact time the camera was triggered by the pulse generator. Three repeated trials were performed for all conditions. The plate drag was found

by first completing a trial without the plate specimen to measure the force of the system. The plate was then added and another trial was completed and the first drag time history was subtracted from the latter in post-processing.

2.5.4 Fluid Flow Surrounding Heaving Flexible Plates

To characterize the fluid dynamics surrounding the flexible plate specimen, particle image velocimetry experiments were performed on the same setup presented earlier in the Hydroelasticity lab. The experiments were completed for frequencies of 0.50 Hz and 0.31 Hz, same as those in the load cell experiments. The smallest h tested was 6.0 cm while the largest value was 18.5 cm. The depth of the plate was limited by the available equipment in this case. The strength of the laser was a driving factor in the lenses that could be utilized for the experiments. Future work will expand upon the conditions tested here. Repeatability was confirmed through repeated trials.

2.6 Uncertainty in Measurement Techniques

The gradient-based edge detection techniques utilized to measure the deflection of the plate utilizes pixel coordinates as explained in detail in Sec. 2.3.2. The accuracy of the algorithm is limited to a the size of a pixel which is derived from the calibration of the camera. The white light experiments presented in Sec. 3.1 and Sec. 3.2 retain accuracy to 0.027 centimeters which corresponds to the calculated length of a single pixel. The strain gauge load cell has a sensitivity of 2 mV/V. Utilizing the calibration factor from the manufacturer, the sensitivity is equivalent to 0.25 Newtons. PIV results have been analyzed for both instantaneous velocity uncertainties as well as instantaneous correlation values. The instantaneous uncertainty has

been calculated for a heaving frequency of 0.5 Hz 18.5 cm below the free surface after completing a multi-pass analysis with 4 passes. Fig. 2.9 shows a non-dimensional time history of the instantaneous uncertainty. At times, sparse uncertainties arise that reach the full-scale flow velocity. The localized regions where this occur are considerably small in comparison to the testing window, and do not remain in the same location as time steps progress. The sparse nature of the uncertainties as well as the inconsistency in the location of the high uncertainties leads to the determination that the results may be analyzed with confidence that the flow velocity is being captured accurately. The instantaneous correlation value also suggests that the results are accurate to the flow. A correlation value of 0.5 is considered to be a strong correlation with 0.4 referring to a good correlation. Throughout the time history of a single oscillation, the correlation value throughout the testing window remains high with any correlation value above 0.5 shown in red in Fig. 2.10.

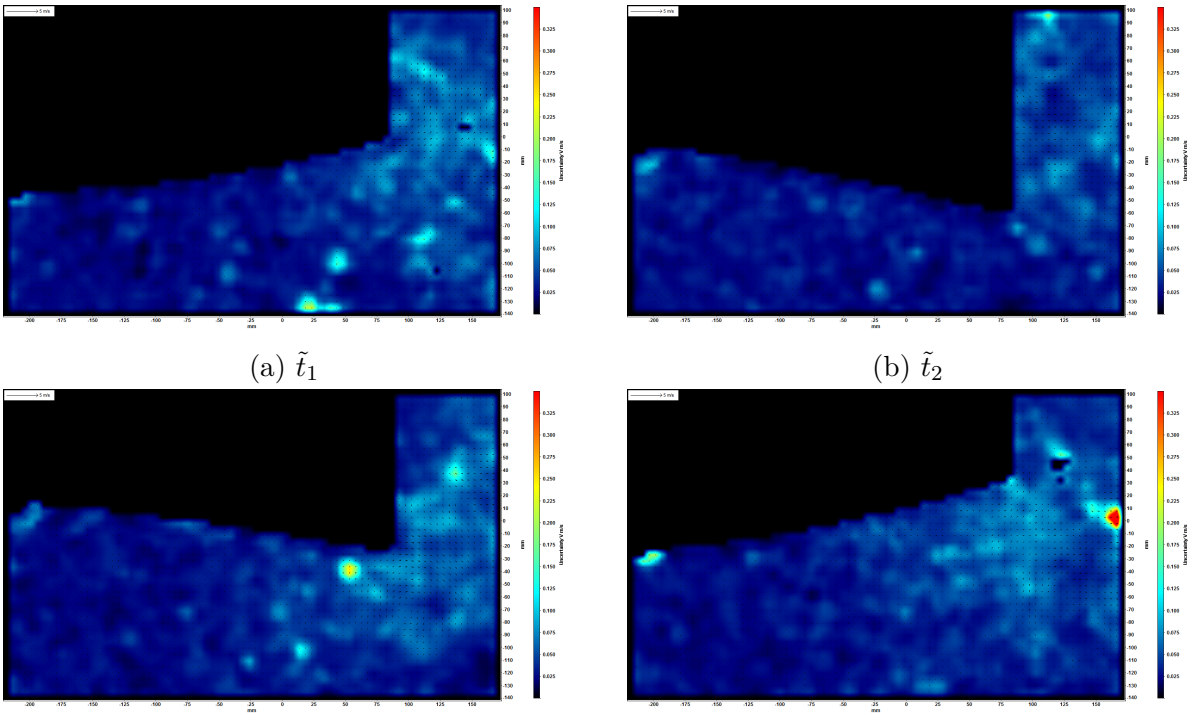

(a) $\tilde{t}_1$ (b) $\tilde{t}_2$

(c) $\tilde{t}_3$ (d) $\tilde{t}_4$

Figure 2.9: Instantaneous flow velocity uncertainty at f = 0.50 Hz and h = 18.5 cm.

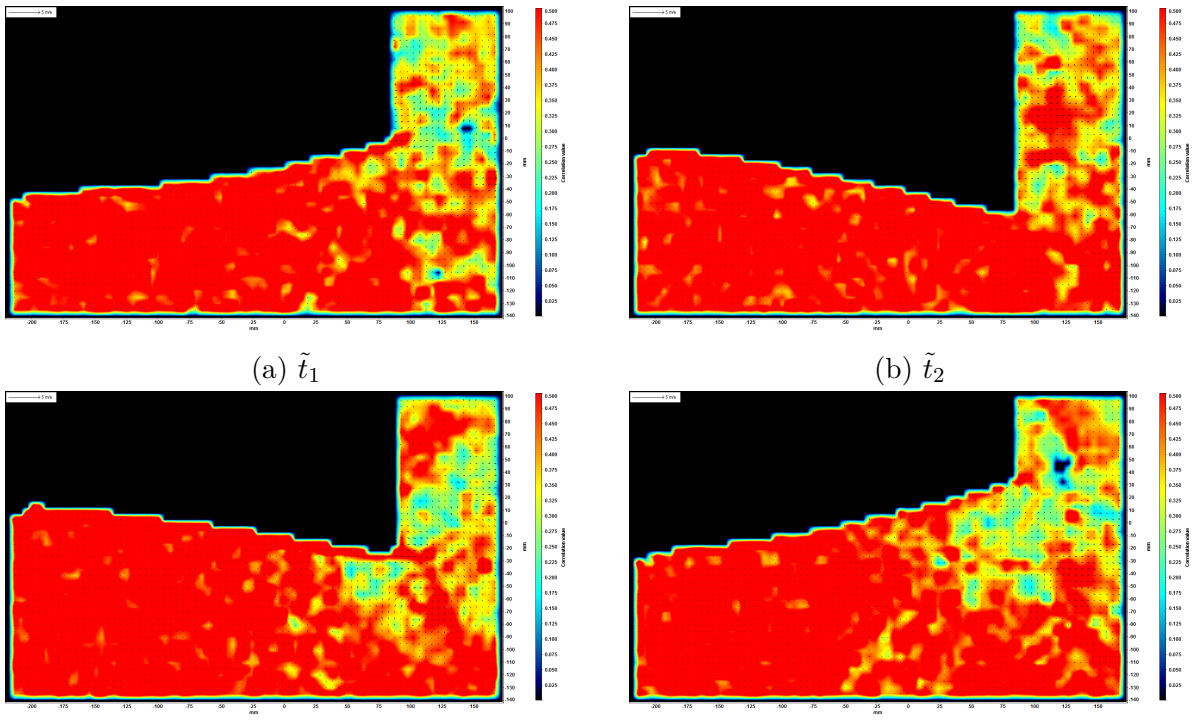

(a) $\tilde{t}_1$ (b) $\tilde{t}_2$

(c) $\tilde{t}_3$ (d) $\tilde{t}_4$

Figure 2.10: Instantaneous correlation value at f = 0.50 Hz and h = 18.5 cm.

Chapter 3

Results and Discussion

The results from the experiments described in the previous section are summarized in this chapter. They are laid out as follows: Sec. 3.1 shows the results of the experiments investigating the effects of proximity to the free surface for a flexible plate oscillating at constant frequency, Sec. 3.2 shows the results of experiments focused on investigating the effects of varying the oscillatory heaving frequency on plate deformations, Sec. 3.3 discusses the fluid loads measured on flexible plates at varying heaving frequencies and heights to the free surface, and Sec. 3.4 presents the results of PIV experiments showing the fluid flow around the flexible plate specimen.

3.1 Effect of Proximity to the Free Surface on Reconfiguration for a Flexible Plate Under Prescribed Constant Frequency Oscillatory Motion

The investigation of free surface effects was initiated with experiments that kept the prescribed heaving frequency constant while varying the proximity to the free surface, h. Each trial was conducted in accordance with the experimental matrix described in Table 2.1. This section will present and discuss structural dependence on proximity to the free surface, symmetry in the plate deflection, and the tip kinematics of the controlled heave experiments

under constant heaving frequency with varied proximity to the free surface.

3.1.1 Structural Response Dependence on Height to the Free Surface

A systematic approach was taken in selecting the h values that were tested. Six evenly spaced heights in intervals of 5 cm were originally tested and the dynamic plate deflection was measured with a high-speed camera. A seventh height to the free surface was then added to better characterize the region close to the free surface once the location in which free surface effects act on the plates was found. Table 3.1 shows the average heights to the free surface that were tested along with the corresponding line color which will remain consistent for the remainder of the section. The sinusoidal time-history of the keel, measured by the string potentiometer, is shown in Fig. 3.1 for the seven different h values, where zero corresponds to the undisturbed free surface. The results show that the motion prescribed to the heaving plate was repeatable independent of the height to the free surface or other factors within the experimental setup. Multiple trials were completed at each h value and the repeatability of those results are shown in Appendix A.1. It is important to note that the deeper h values are plotted in darker colors and as h decreases, the color lightens as seen in the legend below. This will hold true for the rest of this section.

The heaving frequency was kept constant at 0.5 Hz for this set of experiments. The time range of data acquired was at steady-state, so any transients associated with the motor startup are not captured. The minimum keel distance to the free surface, corresponding to the crests in Fig. 3.1, was utilized to synchronize the position and camera data. The time index of the minimum keel height was used to find the adjacent frame in the camera data. The time index was taken as the initial time interval and the rest of the data was shifted

Table 3.1: Constant Frequency Experiments Line Styles

h (cm)	Line
5.3	
8	
10.6	
15.5	
20.5	
25.5	
30.5	

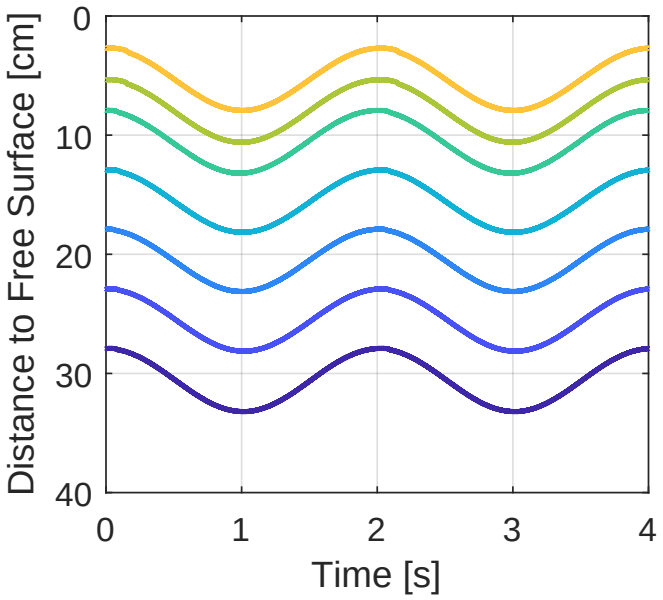

Figure 3.1: Time history of keel location in reference to the undisturbed free surface at varying h values.

accordingly.

The maximum and minimum keel positions of each trial were utilized as time instances to compare the deformed plate shapes at varying depths in the water column. At the maximum keel depth for each trial, a change in the deformed plate shape is apparent as h decreases, and the plate approaches the free surface. Fig. 3.2 shows the deformed plate shapes of one trial at each depth with X corresponding to the horizontal distance beginning at zero

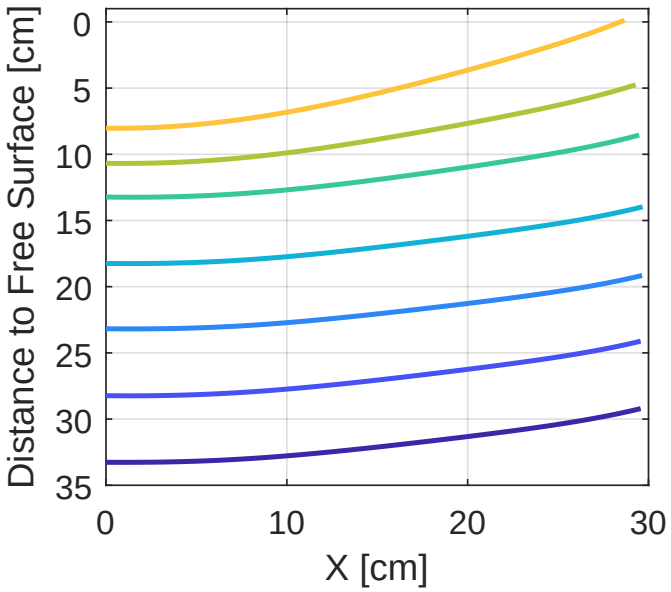

Figure 3.2: Deformed plate shapes at the maximum keel depth for all h values.

corresponding to the start of the unsupported length of the plate. The y-axis shows the global position of the plate, with zero corresponding to the undisturbed free surface and increasing with increased distance from the free surface. It can be seen that deformation at the free edge of the plate significantly increases as the plate depth decreases, specifically at h values of 5.3 and 8.0 cm.

The same comparison can be made at the minimum keel depth for each h value, but the distinct difference in plate deformation is not as easily seen. The plate has larger deformations at the maximum keel depth from the free surface for each run than those at the minimum keel depth. The two varying trends suggest that free surface effects may cause asymmetric deformations depending on the plate proximity to the free surface. Many factors can contribute to the change in deformations such as changes in pressure as the plate approaches the free surface, generation of waves, and even surface tension for cases where the tip of the plate pierces the surface.

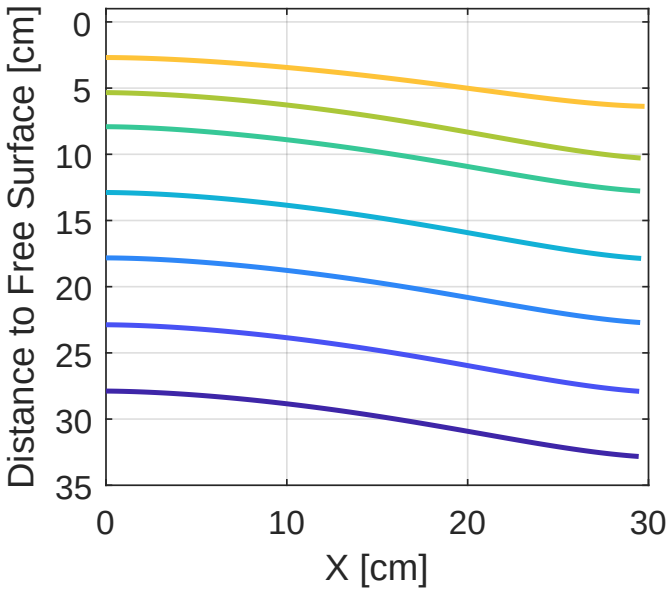

Figure 3.3: Deformed plate shapes at the minimum keel depth for all h values.

3.1.2 Symmetry in Plate Deflection

To better understand and compare the deformed plate shape, the deflection is defined as the difference in vertical position at any point along the length of the plate and the vertical position of the keel. Fig. 3.4 demonstrates the physical meaning of deflection as it has been defined in this thesis. Keeping with the same coordinate system defined earlier, positive deflection corresponds to deflection downward while negative deflection is deflection upward, toward the free surface.

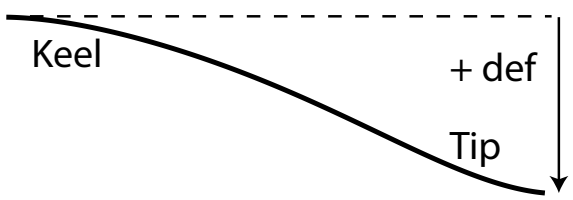

Figure 3.4: Schematic depicting the physical representation of positive deflection.

Fig. 3.5 is a different way of visualizing the deformed plate shapes shown in Figs. 3.2 and

3.3 .The plot was made by subtracting the vertical position of the keel so the deformed plate shapes can be compared with respect to the keel position in a body-fixed frame. This also allows the maximum and minimum keel position to be plotted on the same axes where the maximum keel height results in positive deflection because the deformed plate shape is below the keel position and the minimum keel height results in negative deflection.

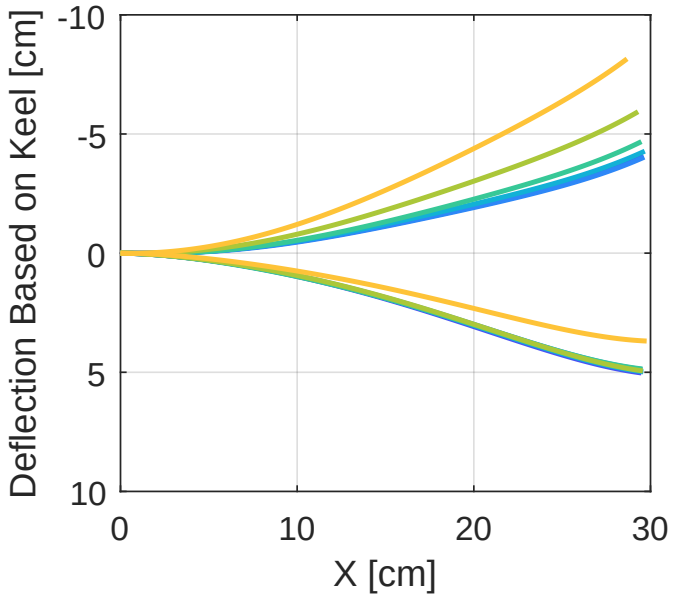

Figure 3.5: Deflection along the length of the plate at all h values plotted in the body-fixed reference frame.

At deep h values, the tip deflection of the plate reaches 5 cm at the maximum keel height, while at the minimum keel height the tip deflection is just lower than 5 cm. This discrepancy is thought to be caused by initial plastic deformation in the plate and investigations will be discussed in Chapter 4 which will confirm the source of this discrepancy. The deepest three heights from the free surface corresponding to h values of 30.6, 25.5, and 20.5 cm show nearly identical behavior when deflecting towards and away from the free surface. At an average height, h, to the free surface of 15.5 cm shown in light blue, the deflection of the plate when the deformation is toward the free surface, the top set of curves, shifts slightly, showing more

deflection than those deeper in the water column, almost as if the tip tends to be attracted towards the free surface. This trend continues for the remaining three h values with the deviation becoming more pronounced as h decreases.

While the change in deflection is gradual when deflection is negative, the top set of curves, a different trend is apparent when analyzing positive deflection, the bottom set of curves. All but the closest condition to the free surface collapse onto one another. This shows that the deflection is identical along the length of the plate for all heights except the trial closest to the undisturbed free surface. The asymmetric deflection of the plate depending on the proximity to the free surface suggests that ***free surface effects do not act uniformly on the plate at all heights*** in the water column and, in fact, have larger effects on the plates which are closer to the free surface and are deflecting towards the free surface rather than away from the free surface.

3.1.3 Plate Tip Deflection and Kinematics

In order to examine the plate kip kinematics more closely, the highest and lowest h value conditions from the constant frequency experiments were assessed. Fig. 3.6 depicts the time history of the tip deflection for h of 5.3 cm and 30.6 cm in yellow and purple respectively. The zero on the vertical axis in the figure corresponds to the undisturbed free surface. It is noted that the sinusoidal waves look somewhat similar and somewhat different. To take a closer look, h for each case is subtracted from the tip position (from Fig. 3.6) and the resulting relationship can be seen in Fig. 3.7. The comparison is seen more clearly in terms of the shape, amplitude, and temporal shift. It can be noted that similar values for the amplitude of each respective time history of deflection is seen. A vertical shift in the tip deflection is seen in the condition closest to the free surface which depicts the asymmetry

seen previously in Fig. 3.5. The asymmetry shows larger deflections towards the free surface than when the plate returns deeper in the water column.

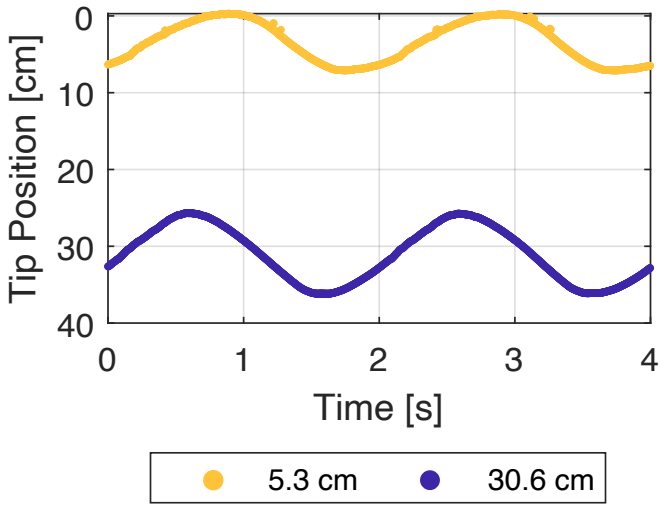

Figure 3.6: Time history of the tip position corresponding to conditions closest and furthest from the undisturbed free surface.

The behavior of the smallest h condition seen in yellow differs from the largest h condition in purple in both amplitude and phase. The 30.6 cm case retains nearly symmetric deflections both towards and away from the free surface where the amplitude of deflection is nearly identical. A phase shift is also observed between the two conditions. It is important to note that Fig. 3.7 only corresponds to the tip of the plate which shows the asymmetry in deflection and phase shift. Earlier, Fig. 3.1 presented the prescribed oscillatory motion which shows the forced oscillatory motion from the motor had constant frequency and amplitude for all conditions.

Figure 3.8 shows the time history of the tip and keel velocities corresponding to the smallest h case (shown as the yellow dot in Fig. 3.9). The keel motion represents the prescribed motion directly from the motor. The motion of the keel is approximately 90 degrees out of

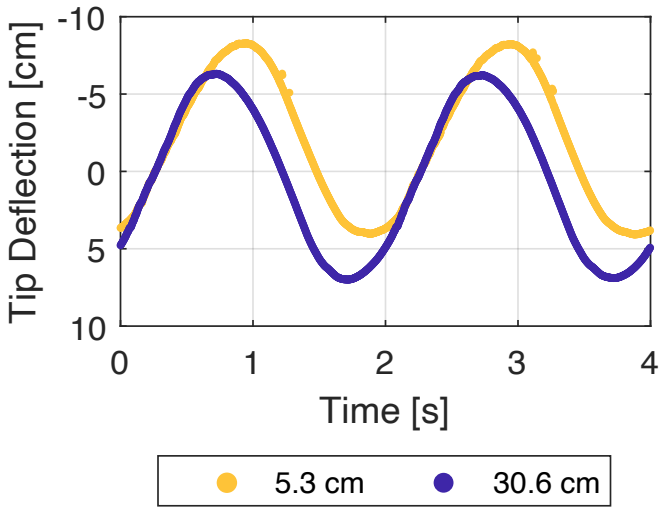

Figure 3.7: Time history of the tip deflection corresponding to conditions closest and furthest from the undisturbed free surface.

phase with the motion of the plate tip when the plate is closest to the free surface. As the keel moves down in the water column, the tip of the plate is ascending and when the keel moves up in the water column the tip of the plate again does the opposite. The tip velocity curve shows similar asymmetry to the tip deflection as the plate reaches higher velocities as the plate returns deeper in the water column in comparison to when the plate reaches the free surface. Noting that deflection has been defined as the difference between a point along the length of the plate and the keel position at any instant, two aspects are present in the deflection. The first aspect is the reconfiguration of the plate under the hydrodynamic loading while the second is rigid body motion from the keel moving opposite the plate tip.

Isolating the tip position of each h value at a single frame when the keel is furthest from the free surface, the tip deflection may be plotted against the average height to the free surface, h, as seen in Fig. 3.9. Analysis of the tip deflections at varying h depicts an asymptotic trend as plate depth increases. The behavior suggests that there is a critical depth for the

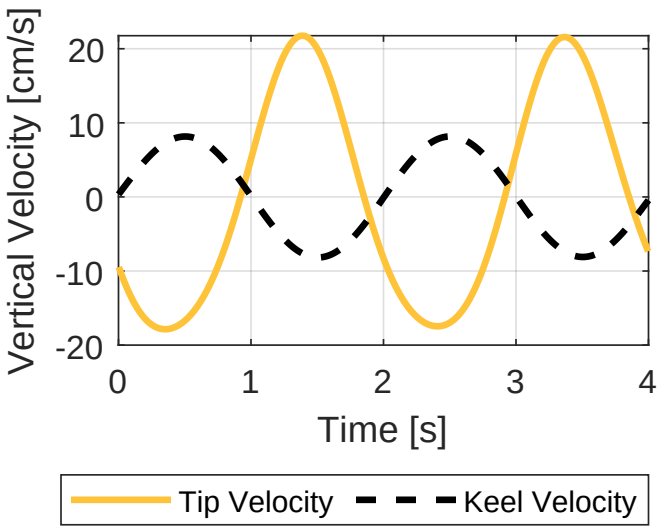

Figure 3.8: Plate tip and keel velocity time histories for a h value of 5.3 cm.

specific prescribed heaving frequency of 0.5 Hz that distinguishes deep water behavior from shallow water behavior. This is the threshold that the free surface effects become important to note when analyzing the passive reconfiguration of the flexible plate. When h is small, the tip deflections are large and when h increases, the tip deflections approach 4 cm.

3.2 Effect of Varying Frequency of Prescribed Oscillatory Motion on the Passive Reconfiguration of a Flexible Plate

After analyzing the effects of proximity to the free surface on the structural response of the flexible plate, attention was shifted to the effects of varying the frequency of the prescribed oscillatory heaving motion. The same testing procedures presented in Sec. 3.1 were followed to complete the variable prescribed heaving frequency experiments, with additional frequen-

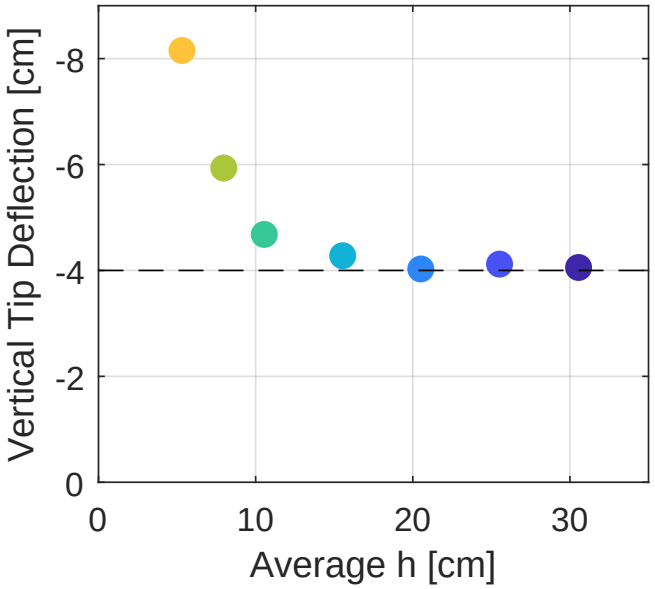

Figure 3.9: Tip deflection at maximum keel depth for varying h values.

cies tested. This section will discuss the effects of varying the heaving frequency of a flexible plate in close proximity to a free surface. A discussion of the dimensional analysis will be followed by preliminary non-dimensional analysis derived from Buckingham Pi theorem.

3.2.1 Dimensional Results

The flexible plate was forced to heave in a sinusoidal fashion by the Nema 23 stepper motor. The heave frequencies were 0.5 Hz, 0.44 Hz, 0.38 Hz, and 0.31 Hz. A time history for each frequency and h value tested can be seen in Fig. 3.10. Note that Table 3.2 shows all h values tested for the varied frequency experiments along with the corresponding line style. The line styles will hold constant for the remainder of the section. Analyzing a single oscillation shows that the heaving motion of the keel is regular and repeatable. This is important since it validates the consistency of the prescribed motion at the keel across all trials.

Table 3.2: Varied Frequency Experiments Line Styles

h (cm)	Line
6	
9	
12	
15	
18.5	
30.5	

The period of oscillation for each of the frequencies varies, getting longer with a decrease in frequency. For the basis of comparison, keel height was used as a matching condition between runs. Taking the time instant of each respective frequency in which the keel reached its maximum depth, the reconfigured plate shapes may be compared. Fig. 3.11 shows the deformed plate shapes at the maximum keel height. The amount of deflection decreases from the highest frequency of 0.50 Hz to 0.44 Hz, but very similar trends are observed where the two heights closest to the free surface deflect at a greater magnitude than those deeper in the water column. The four lower heights deflect at a very similar magnitude.

For a heaving frequency of 0.38 Hz, the plate, which is 30.5 cm below the free surface, begins to deflect less than all other plates. ***This suggests that lower frequencies can impact the point in which deep water behavior occurs.*** Deep water behavior dictates the threshold where free surface effects need to be accounted for. At 0.38 Hz, the deepest plate shows little to no deflection. However, the slowest heaving plate at 0.31 Hz has a unique trend where the deepest four plates deflect away from the free surface. This is opposite to the trends which have been observed for the experiments described in the last section at the largest h values. The plate retained some initial deformation before the experiments were conducted. The deformation is likely due to how the material was stored prior to being shipped. The initial deformation affects the experimental results. Material testing will be conducted to quantify the initial deformation. The initial deformation does not explain the

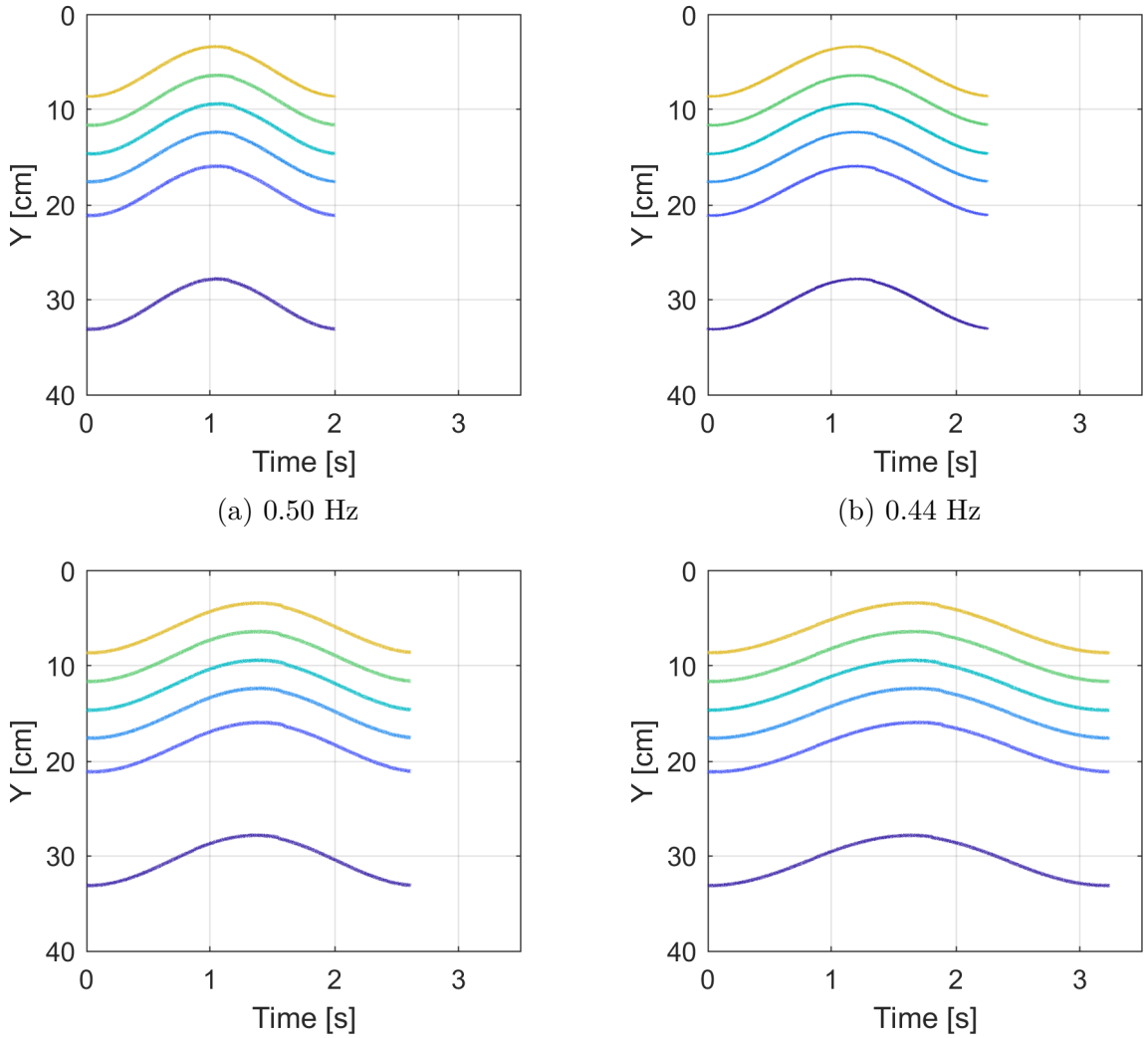

(a) 0.50 Hz

(b) 0.44 Hz

(c) 0.38 Hz

(d) 0.31 Hz

Figure 3.10: Keel heaving history with reference to the undisturbed free surface for prescribed heaving frequencies of a) 0.50 Hz, b) 0.44 Hz, c) 0.38 Hz, and d) 0.31 Hz.

increase in negative deflection at deeper h values, which will require more experiments at lower frequencies to fully define. At low frequency, the tip of the plate moves in phase with the keel due to low maximum velocities. Without free surface effects, no change in plate shape is seen, but as the plate approaches the free surface, the change in pressure on the top-side of the plate creates a suction-like effect and causes defection upward.

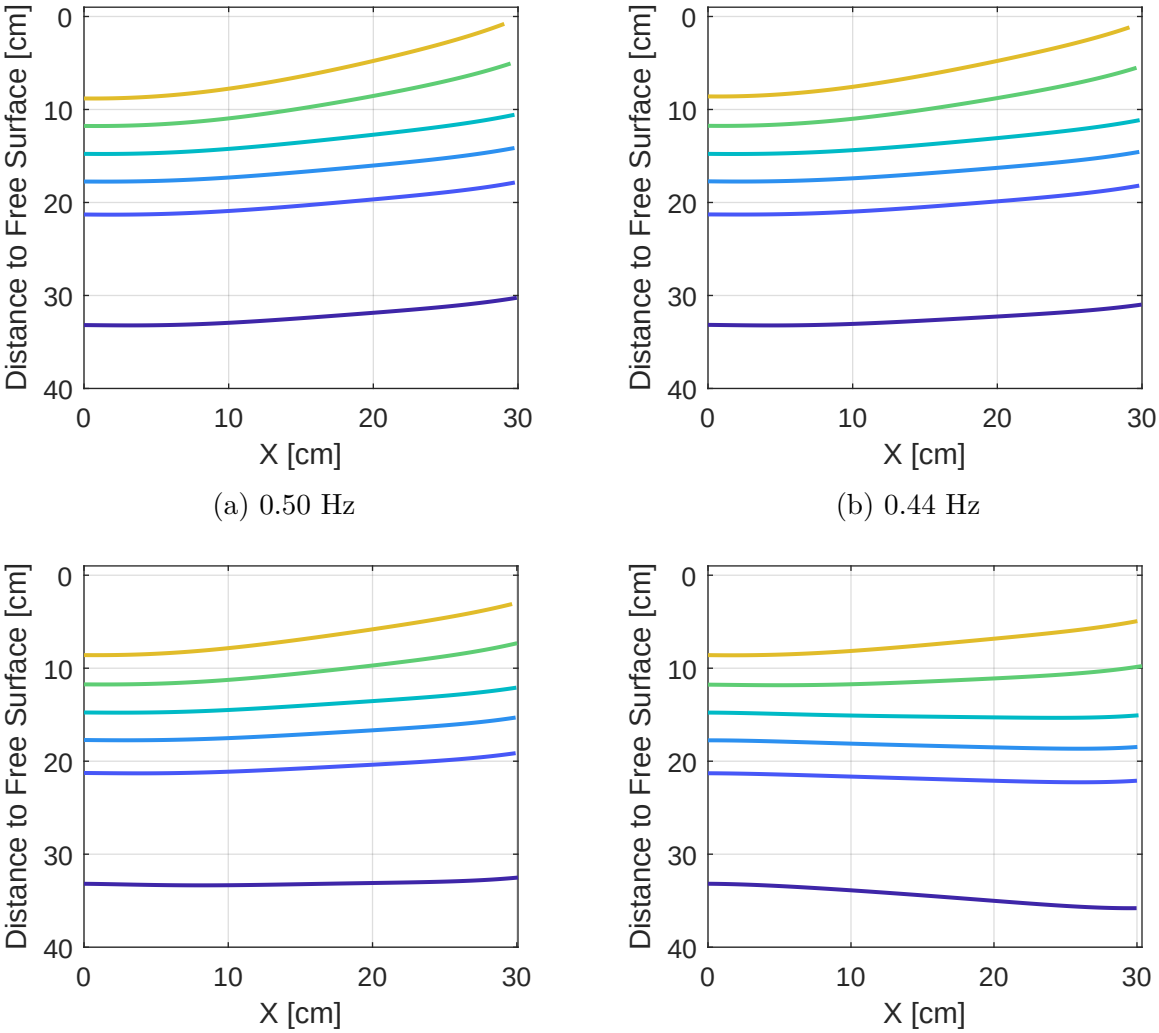

(a) 0.50 Hz

(b) 0.44 Hz

(c) 0.38 Hz

(d) 0.31 Hz

Figure 3.11: Reconfigured plate shapes at the maximum keel height for frequencies of a) 0.50 Hz, b) 0.44 Hz, c) 0.38 Hz, and d) 0.31 Hz.

3.2.2 Non-Dimensional Analysis

Instead of deformed plate shape, deflection along the length of the plate may be analyzed. Fig. 3.12 presents the deflection non-dimensionalized by the tip deflection of each trial for the four tested frequencies and the distance along the plate non-dimensionalized by the length of the plate. The reconfigured shapes correspond to the time when the keel is at its

maximum depth. The higher frequencies of 0.50 Hz, 0.44 Hz, and 0.38 Hz collapse well for each frequency respectively. The lowest frequency shows the plate shapes do not collapse. When looking at the maximum deflection versus submergence, h, in Fig. 3.13, it is evident

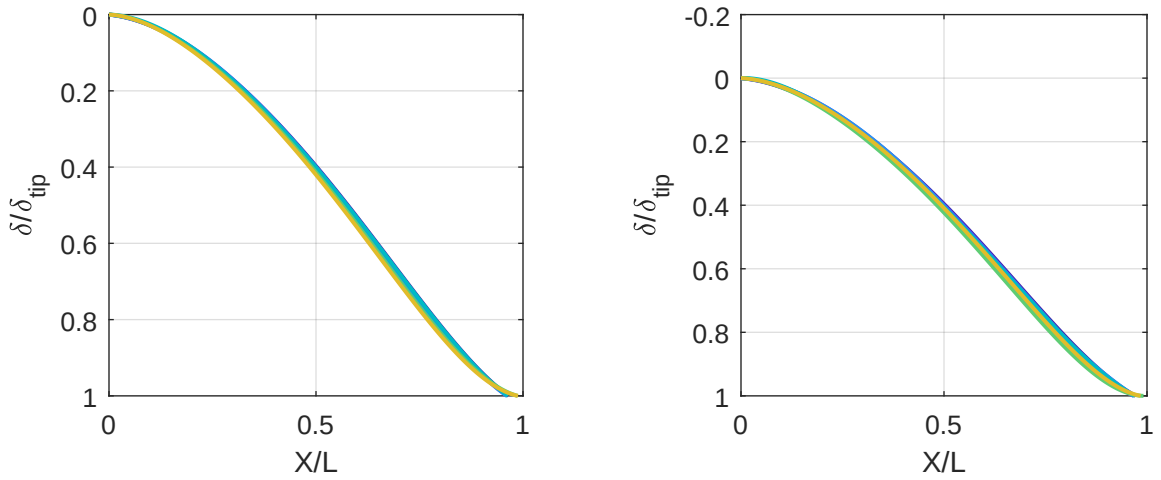

(a) 0.50 Hz

(b) 0.44 Hz

(c) 0.38 Hz

(d) 0.31 Hz

Figure 3.12: Dimensionless plate reconfiguration for frequencies of a) 0.50 Hz, b) 0.44 Hz, c) 0.38 Hz, and d) 0.31 Hz at maximum keel depth.

that each frequency asymptotes to a slightly different non-dimensional value. Since each frequency asymptotes to a different non-dimensional value, a dependency on frequency is evident. The dependence will dictate where deep water behavior occurs and thus, the plate

will deflect in the same fashion independent of increasing depth. At low frequency and deep depth, the asymptotic trend seems to break down. This may stem from the reasoning stated earlier, where the initial plastic deformation of the plate has not been taken into account as well as the velocities reached at the lowest frequency are not significant enough to cause the plate tip to move out of phase with respect to the keel.

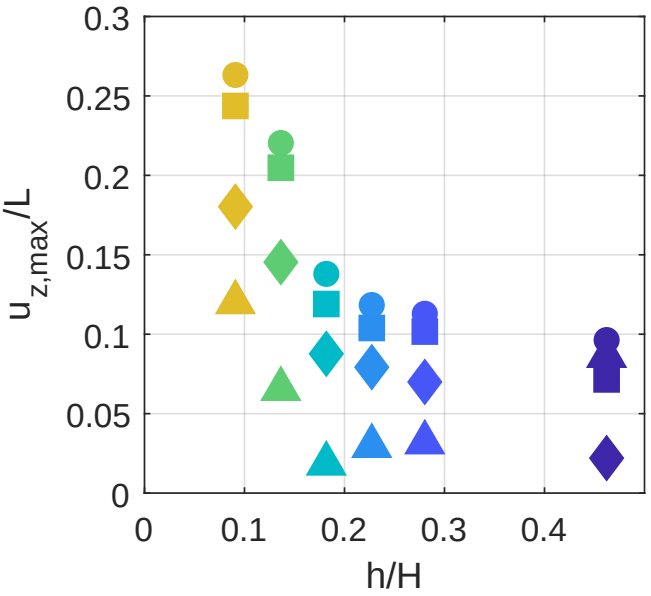

Figure 3.13: Dimensionless maximum deflection across various frequencies and submergence heights.

Frequency may be accounted for by changing the dimensionless parameter. Strouhal number, in this case, accounts for the heaving frequency, heaving amplitude, and maximum velocity of the prescribed keel motion. The Strouhal number presented here is an adapted dimensionless parameter which normally utilizes the constant free stream velocity. Fig. 3.14 shows dimensionless deflection versus Strouhal number for each respective frequency. In this case, because the Strouhal number is dependent upon the frequency of the prescribed oscillatory heaving frequency, we can see a linear relationship between the maximum deflection and oscillation frequency. Further analysis and dimensionless parameters are needed to collapse

these curves, which will lead to a strong understanding of the physics of the problem.

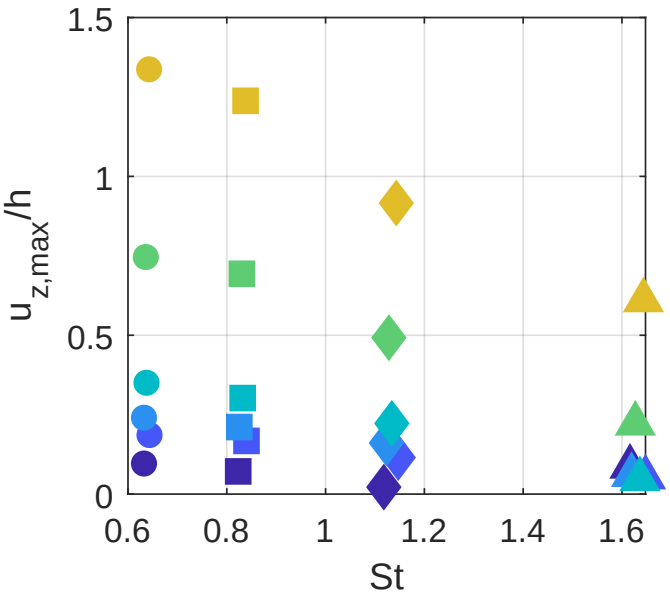

Figure 3.14: Dimensionless maximum deflection versus Strouhal number across frequencies and h values.

3.3 Fluid Loading on Heaving Flexible Plates

The drag force on a very flexible structure can be difficult to measure, but is essential to the understanding of how reconfiguration and flexibility affect fluid flow around deforming bodies. A load cell was placed on the experimental rig to measure the fluid load on the heave post. The plate drag was estimated using this measurement as discussed in this section. Furthermore, a comparison between different frequencies of the prescribed heaving motion as well as various proximities to the free surface, h, are also presented.

3.3.1 Plate Drag

The load cell, which was designed to be integral to the heave post, sampled the tension and compression loads between the plate specimen and DC motor. The experimental setup was designed to slide on linear slides that reduce the resistance of the system, but friction still exists between the plastic of the linear slides and the aluminum T-slot framing. In order to isolate the plate drag from the total force, the load cell measurements were taken without the plate attached so a measurement of the friction in the system could be made. This was done at each h and motor frequency. Then, the experiment was run with the plate attached, and the plate drag on both sides of the keel was assumed to be the total drag measured in the plate experiment minus the forces measured when the plate was not attached. Fig. 3.15 shows the unfiltered data for an average height to the free surface of 6.0 cm and a frequency of 0.31 Hz.

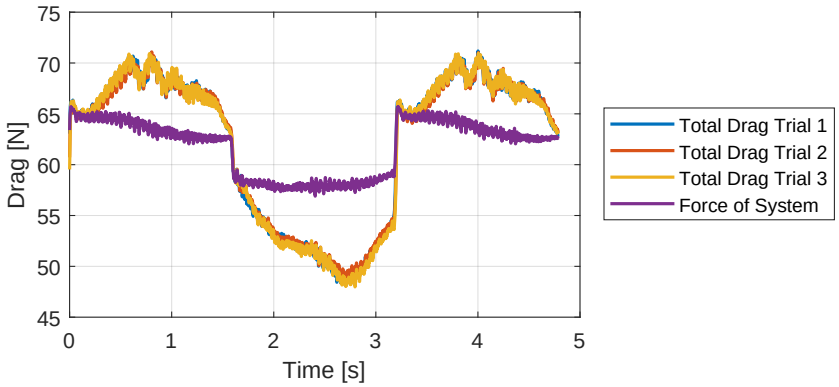

Figure 3.15: Unfiltered drag data for three trials with plate specimen and one trial without the plate specimen.

The drag data was filtered by first completing a fast Fourier transform to analyze the signal within the frequency domain. The frequency domain shows the range of frequencies that are seen in the signal, along with the amount of readings at those frequencies. Many filters were tested and a Butterworth filter was ultimately selected to filter the data. Fig. 3.16a

shows the unfiltered data in black with the filtered data in yellow to justify the selection of this filter. The fast Fourier transform revealed that most of the data occurs below 1 Hz, and very little signals are found above 5 Hz which is seen in Fig. 3.16b. For this reason 5 Hz was selected as the cutoff frequency with which a low pass filter was applied. The key characteristics that stem from the physics of the problem are captured while still filtering out the noise. The filter was applied both before and after averaging the repeated trials together without any difference in the resultant drag being noted.

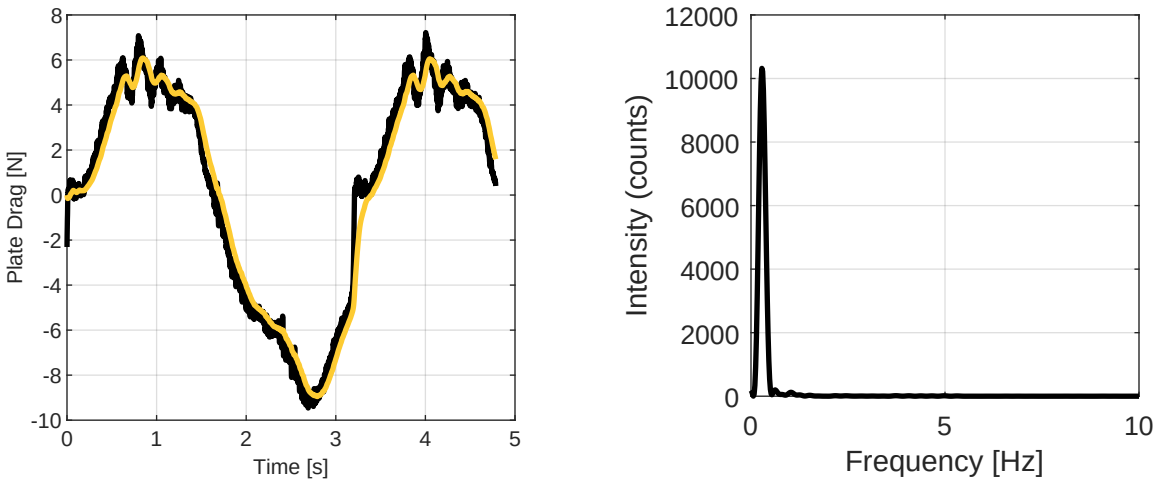

(a) Butterworth Filter (b) Spectral Analysis

Figure 3.16: The (a) raw data (—) and filtered data (—) of the plate of one trial and (b) spectral analysis of the frequency domain.

Four different conditions were tested: the maximum and minimum h values correspond to the maximum and minimum values tested in the varied frequency experiments. The frequencies tested here also correspond to the maximum and minimum frequencies tested in the experiments discussed in Sec. 3.2. Fig. 3.17 depicts the time history of the keel position on the left axis shown in black, and the time history of the plate drag on the right axis shown in yellow. When comparing flexible plates at the same height but varying frequencies, runs taken at lower frequency experience approximately equal drag to runs at

higher frequency. One aspect that leads to the drag not increasing for the higher velocities seen with the plate heaving at a higher frequency is reconfiguration. From the varied heaving frequency experiments, the reconfiguration is much greater in the 0.50 Hz heaving plate than the plate heaving at 0.31 Hz. By reconfiguring more, the plate is able to decrease its area perpendicular to the flow or direction of travel. This conclusion is consistent with the findings of Vogel (1996), Alben *et al.* (2002), and Gosselin *et al.* (2010). While this is true, the problem at hand differs greatly due to the unsteady nature of the prescribed heaving motion. The oscillatory motion requires the plate to return to its original position at some point throughout the period of oscillation. The total projected area perpendicular to the direction of the flow changes as the plate moves. When the projected area is lower, it is expected that the drag force is lower as compared to times when the projected area is higher. As velocity increases, drag is also expected to increase. Since an increase in drag is not seen with the increased velocity, the change in projected area contributing to decreased added mass effects impact the drag more than the change in velocity. Added mass effects are being seen since the body is constantly accelerating and decelerating in the fluid. The body that heaves at a higher frequency reconfigures to a larger degree, which decreases its projected area. The plate heaving at a lower frequency does not have increased deformations and the fluid above the plate is trapped, creating a no slip condition. Sec. 3.4 will further show that the fluid surrounding the plate heaving at a higher frequency flows at a greater rate over the plate, escaping over the plate edge. The lower heaving frequency does not reconfigure to the same degree and is forced to displace larger amounts of fluid throughout the period of oscillation.

Fig. 3.18a compares both h values of 30.5 cm (purple) and 6.0 cm (yellow) at a heaving frequency of 0.50 Hz while Fig. 3.18b shows a comparison of both h values at a heaving frequency of 0.31 Hz. When the plates are far away from the free surface, the drag time

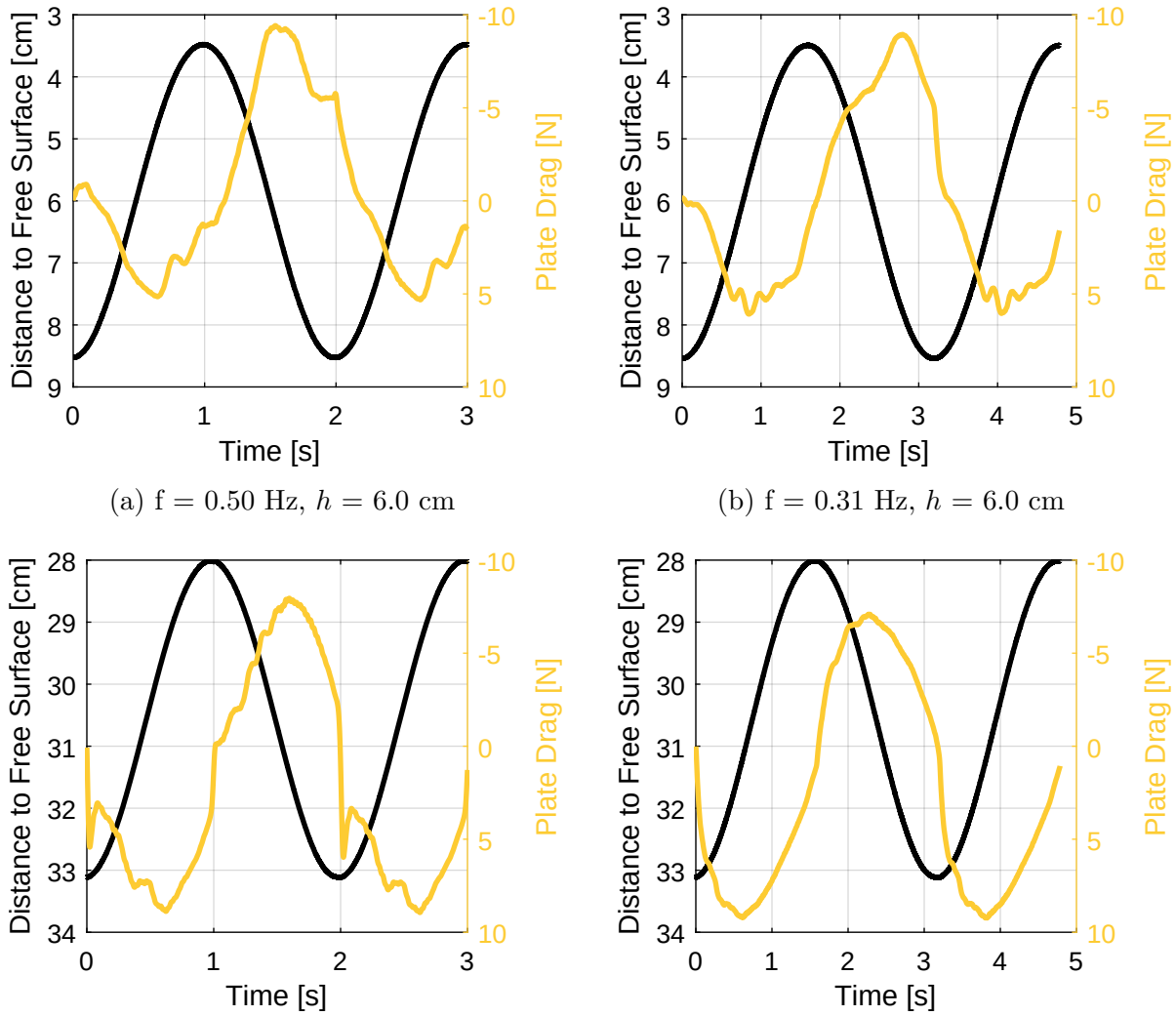

(a) f = 0.50 Hz, h = 6.0 cm

(b) f = 0.31 Hz, h = 6.0 cm

(c) f = 0.50 Hz, h = 30.5 cm

(d) f = 0.31 Hz, h = 30.5 cm

Figure 3.17: A time history of plate drag (—) and keel position (—) for various heights to the free surface and frequencies.

history is almost symmetric about zero, or symmetric in terms of the compression and tensile loads. Some discrepancies exist from plastic deformation existing in the plate prior to experiments. For the current setup, compressive loads are found when the plate moves away from the free surface, while tensile loads occur when the plate approaches the free surface. The drag time history curves shift upward when h is 6.0 cm for both frequencies shown. The shift upward in the plate drag corresponds to more drag on the plate when it moves

downward at low h values. At this instant, the keel is moving deeper in the water column and the plate is deflected towards the free surface. The overall crest to trough amplitudes is similar for the respective frequency, independent of h. A reduction in drag is seen as the plate approaches the free surface, which is consistent with the decrease in deflection seen in earlier experiments. The shift in drag can be attributed to a decrease in pressure above the plate as it approaches the free surface. The plate is required to displace less fluid throughout the heaving motion and thus is not experiencing the same added mass effect that is seen deep in the water column. When the flexible plate returns deeper in the water, less pressure is acting on the top of the plate while it pushes through the water which causes an increase in drag.

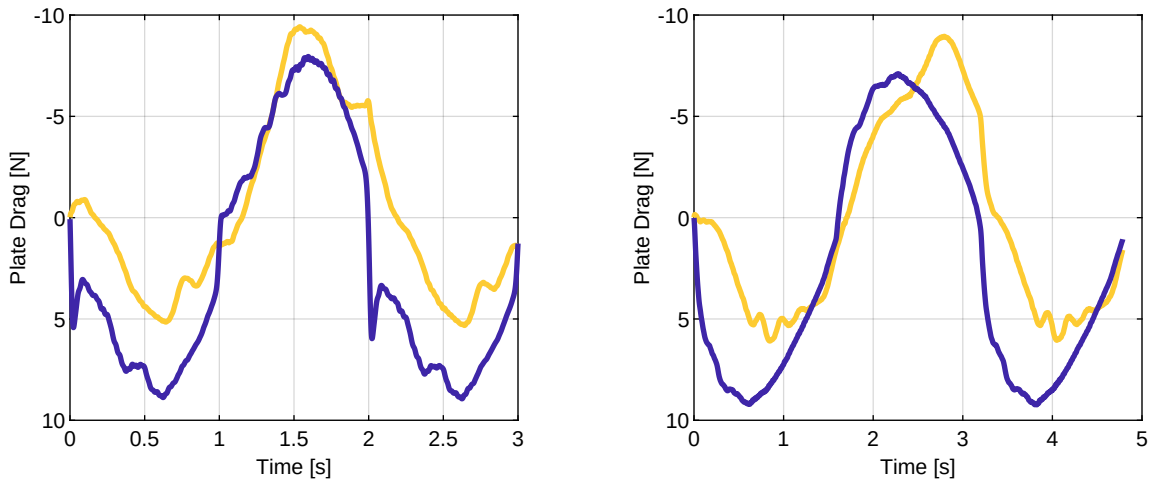

(a) f = 0.50 Hz (b) f = 0.31 Hz

Figure 3.18: Comparison of plate drag at h of 30.5 cm (—) and 6.0 cm (—) at heaving frequencies of a) 0.50 Hz and b) 0.31 Hz.

3.4 Fluid Flow Surrounding Heaving Plates

PIV experiments were conducted in the Hydroelasticity laboratory for proximities to the free surface of 18.5 cm and 6 cm. A height of 18.5 cm was selected to analyze the fluid dynamics of the system exhibiting deep water behavior in contrast to the height closest to the free surface which exhibits shallow water behavior. Both h values were tested at prescribed heaving frequencies of 0.50 Hz and 0.31 Hz. A unique masking technique was developed to best suit the dynamic nature of the oscillatory motion of the plate which will be explained within this section, followed by the velocity field measurements.

3.4.1 Dynamic Masking

Particle image velocimetry requires the specimen within the experimentation window to be masked as well as the area above the specimen because, for the case presented here, the region above the flexible plate is not illuminated. If the entire testing section were to be post-processed, inaccuracies would be incorporated into the interrogation windows and result in velocity fields that are not representative of the fluid flow. Between time steps, the plate moves vertically in the frame due to the prescribed heaving motion. The dynamic motion of the plate required the development of a new dynamic masking technique that has not been seen in literature.

The method used involves a two-step process where images are first post-processed to find the edge of the plate. The edge was then used as the boundary for the mask. Each frame had its own unique mask. One image for each double frame was exported from the DaVis software, which can be seen in Fig. 3.19a. The raw images were imported into Matlab to perform image processing for each frame. The end result of the image processing was a unique mask for each frame or time step. The gradient-based edge detection technique

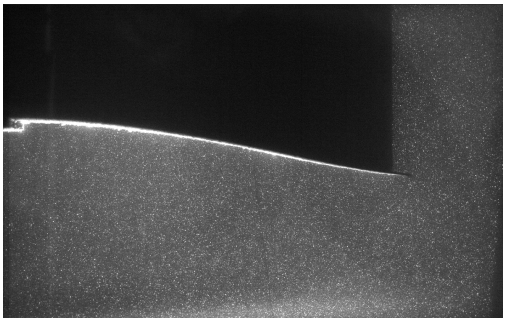

(a) Raw Image

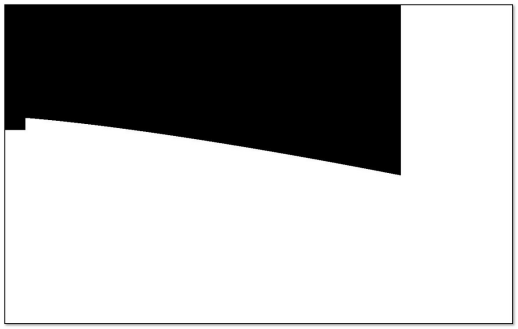

(b) Mask

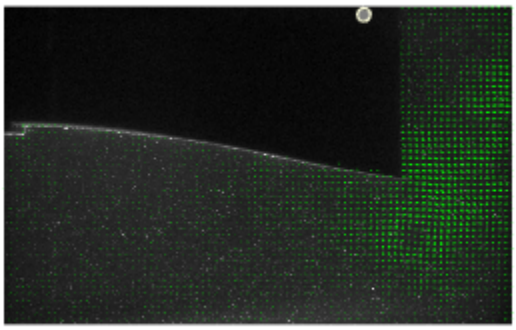

(c) Velocity Vectors

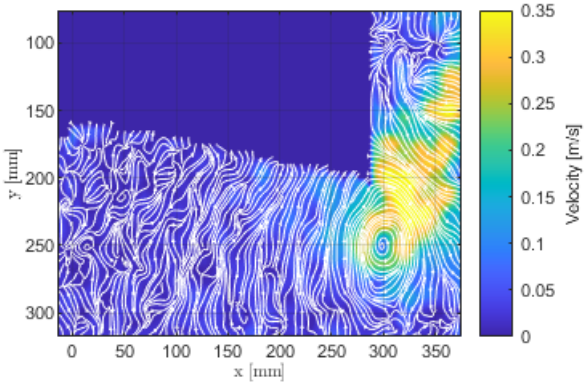

(d) Velocity Field and Streamlines

Figure 3.19: PIV data processing from the a)raw image to the b)masked image which result in the c)velocity vectors and d)streamlines.

utilized the contrast between the illuminated particles seeding the fluid and the dark section above the plate that the laser sheet could not illuminate. For the specific case shown, the laser light sheet always shines underneath the plate. The algorithm was designed to work from the top of the image down toward the plate edge. Once an illuminated pixel was found, it was recorded and a line could be plotted and fit such that it showed the line of illumination seen in the raw image. Based on the line of illumination, a new image was created where all pixels on the line and below it were designated as white. All pixels above the line were designated to be black. An example of one of the created images, which is the mask image,

is seen in Fig 3.19b. The mask images were brought back into the DaVis software and stored as a singular mask file where each frame corresponded to one mask image. Post-processing of the raw videos was completed in DaVis which is seen in Fig. 3.19c to find the velocity vectors and then output to Matlab to show the velocity field and streamlines seen in Fig. 3.19d where the masked regions were not included in the calculations.

3.4.2 Velocity Field and Streamlines

The velocity vector data exported from the DaVis software was utilized to create vector field contours and streamline plots. The dimensionless time parameter, $\tilde{t}$, is the time divided by the period of oscillation for the respective run. Four time instances were selected for comparison which are the maximum keel depth, halfway traversing up, minimum keel depth, and halfway traversing down corresponding to $\tilde{t}_1$, $\tilde{t}_2$, $\tilde{t}_3$, and $\tilde{t}_4$ respectively.

At an h of 18.5 cm, a prescribed heaving frequency of 0.50 Hz was shown to have deep water behavior in the constant frequency experiments discussed in Sec. 3.1. At the deeper h value of 18.5 cm and a heaving frequency of 0.50 Hz, large velocities are seen relative to the other runs in Fig. 3.20. A vortex begins to be shed from the plate at $\tilde{t}_1$ as the plate transitions from a downward motion to an upward motion. The shed vortex is seen at $\tilde{t}_2$ as the fluid on top of the plate accelerates moving left to right from the keel to plate tip. As the plate decelerates at time $\tilde{t}_3$, the fluid being diverted off the plate from the keel to the tip is seen moving significantly faster than the surrounding fluid. When the plate transitions once more and the keel returns to deeper in the water column, the strong vortex that is seen in Fig. 3.20c is shed and seen moving out of frame in Fig. 3.20d. An important observation of the velocity field is that the fluid motion is symmetrical, forming strong vortices from the fluid moving down the plate against the direction of travel before shedding them.

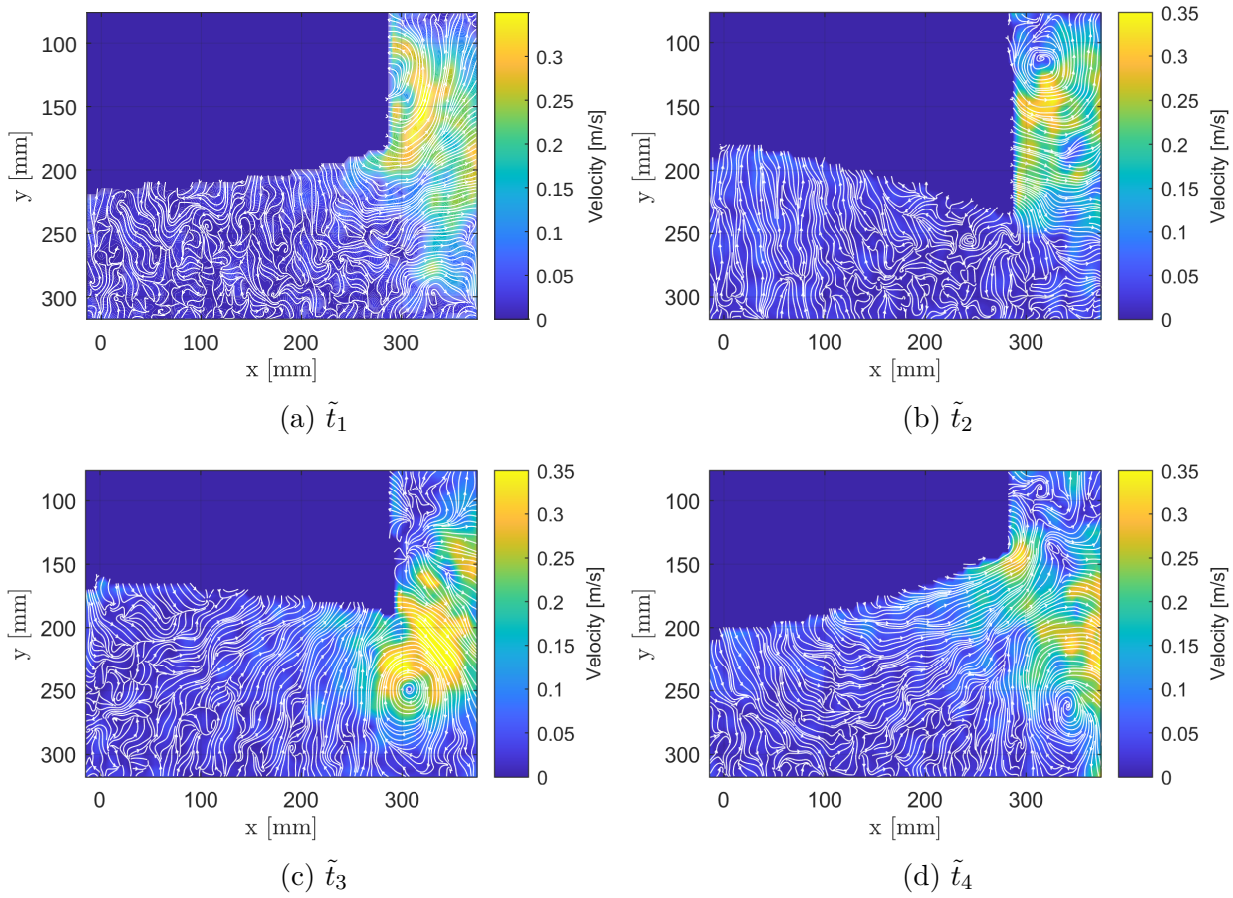

(a) $\tilde{t}_1$ (b) $\tilde{t}_2$

(c) $\tilde{t}_3$ (d) $\tilde{t}_4$

Figure 3.20: Velocity field measurements with streamlines depicting the direction of fluid flow at f = 0.50 Hz and h = 18.5 cm.

The lowest frequency tested, 0.31 Hz, at the same h of 18.5 cm behaves similarly by showing symmetric behavior through its trial. Fig. 3.21a shows a shed vortex moving up and out of the field of view. The vortex seen here is weaker than the flexible plate heaving at 0.50 Hz due to the lower keel and tip velocities of the plate. At the next time step when the keel is accelerating towards the free surface, the fluid moving off the topside of the plate has lower velocity as well. A notable difference in the two cases is that the deflection of the plate is much smaller in the case where the plate is heaving at 0.31 Hz. The decrease in deflection also contributes to less fluid being forced from the keel to the tip of the plate. This results in the plate having to move larger amounts of fluid in its range of motion in comparison to

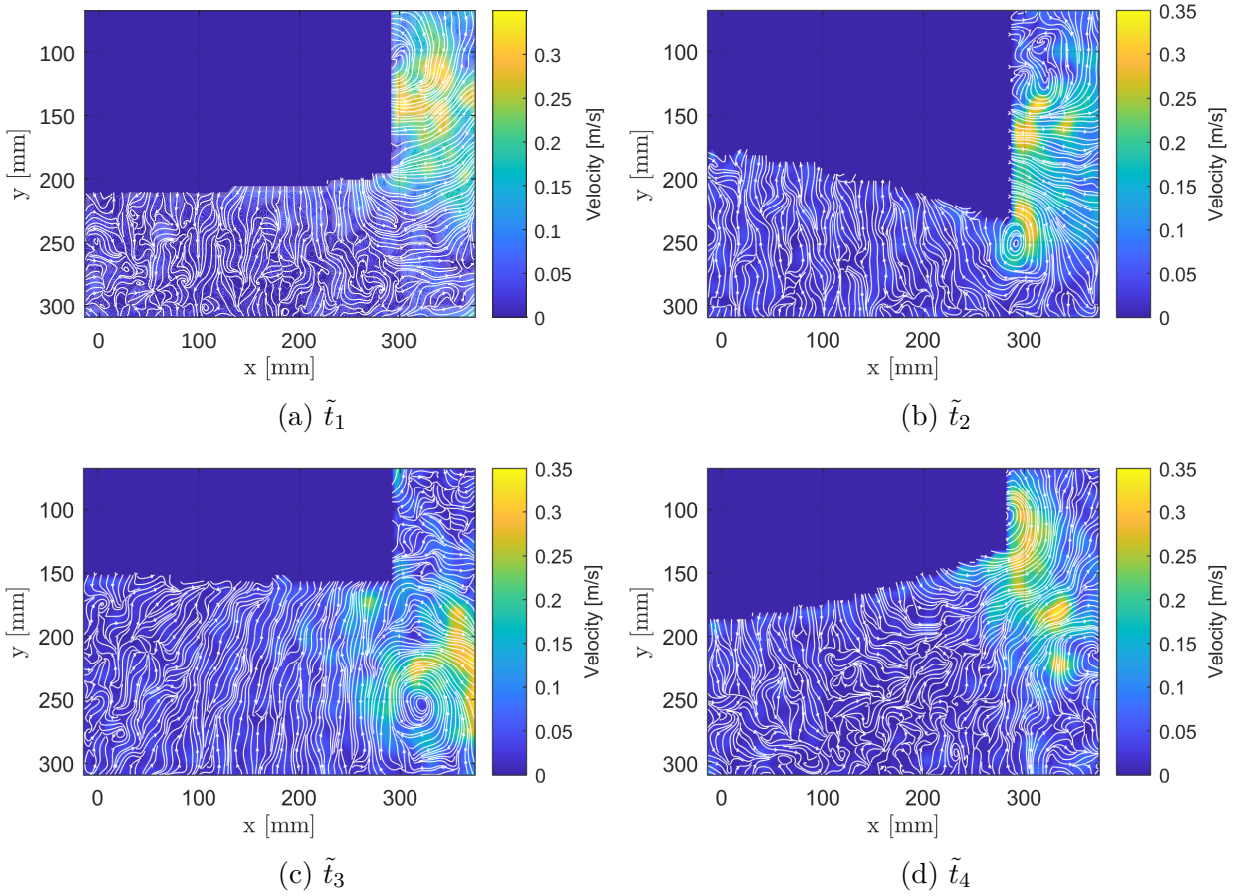

(a) $\tilde{t}_1$ (b) $\tilde{t}_2$

(c) $\tilde{t}_3$ (d) $\tilde{t}_4$

Figure 3.21: Velocity field measurements with streamlines depicting the direction of fluid flow at f = 0.31 Hz and h = 18.5 cm.

the previous case.

When the average keel height is positioned at the closest h value to the free surface of 6.0 cm, the symmetry in the fluid motion around the plate breaks down. Fig. 3.22 shows the case closest to the free surface with prescribed heaving keel motion of 0.50 Hz. At $\tilde{t}_1$, the keel is at its maximum distance from the free surface while the tip of the plate is still at the free surface. As the keel begins to return towards the free surface, the tip starts to move downward, but a vortex is not formed since the keel and tip of the plate are not moving in the same direction. The fluid above the plate is unable to escape over the edge of the plate at the plate tip and this is seen through the low fluid velocities around the plate tip at $\tilde{t}_2$.

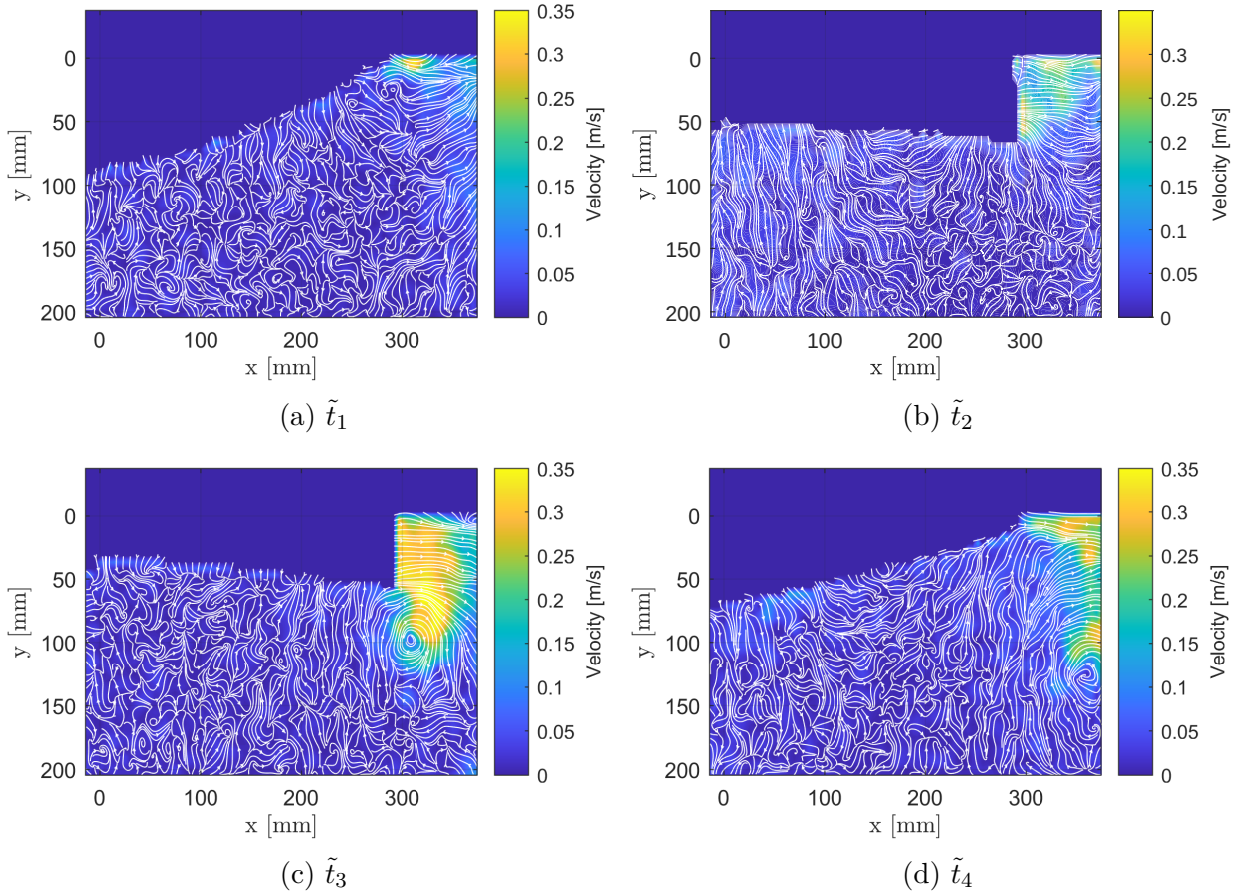

(a) $\tilde{t}_1$ (b) $\tilde{t}_2$

(c) $\tilde{t}_3$ (d) $\tilde{t}_4$

Figure 3.22: Velocity field measurements with streamlines depicting the direction of fluid flow at f = 0.50 Hz and h = 6.0 cm.

When the keel approaches its minimum distance to the free surface, the plate tip accelerates toward the free surface exhibiting a lag effect where the plate tip reaches higher velocities approaching the free surface. As a consequence of the lag effect, fluid is pushed away from the keel at a high rate of speed and a strong vortex is formed. Free surface effects change the motion of the fluid such that the streamlines are seen moving parallel to the free surface. The fluid in this region is forced away from the plate, but not upward toward the free surface and is forced out of the frame which is the direction of least resistance. Ultimately, the vortex is shed as the keel accelerates again moving deeper in the water column.

Fig. 3.23 corresponds to the same h, 6.0 cm, but an oscillatory heaving motion of 0.31 Hz.

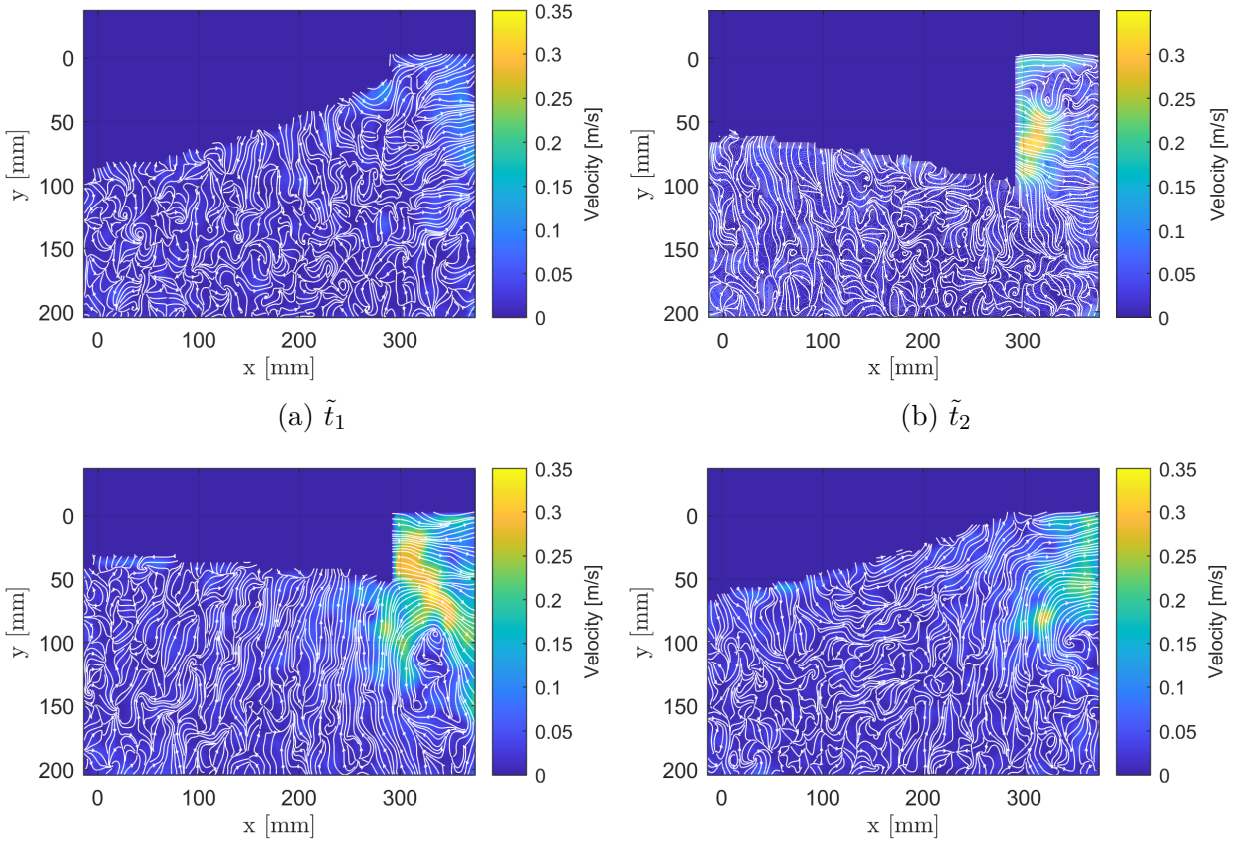

(a) $\tilde{t}_1$ (b) $\tilde{t}_2$

(c) $\tilde{t}_3$ (d) $\tilde{t}_4$

Figure 3.23: Velocity field measurements with streamlines depicting the direction of fluid flow at f = 0.31 Hz and $h = 6.0$ cm.

The decrease in frequency lowers the velocity of the plate which is immediately apparent by the loss in fluid velocity at all time steps. It is important to note that the scaling of the color bar has been shifted slightly for this specific figure due to the decrease in overall velocity compared to the previous figures. Again, similar to the higher frequency case, no vortex is formed close to the free surface. The plate tip lags behind the keel motion and is forced to accelerate back to the free surface at $\tilde{t}_3$. The fluid is forced from the keel to the plate tip and a weak vortex is formed at the plate tip, extending under the plate. As the plate returns to deeper in the water column the vortex is shed and continues out of the frame.

Chapter 4

Conclusions and Future Work

4.1 Conclusions

The fluid-structure interaction of a flexible plate structure heaving near a free surface due to prescribed oscillatory heaving motion has been presented and discussed. White light experiments were conducted to investigate the structural response throughout the heaving event. The white light movies were recorded at various heights to the free surface as well as frequencies to investigate the two factors independently. Image-processing allowed pixel coordinates to be determined that correspond to the deformed plate shape in each frame. A calibration translated the pixel coordinates to laboratory coordinates with length units to measure deflections. White light movies confirmed the repeatability of the structural response with earlier experiments. Further experiments aimed to study the fluid loading on the flexible plate structure utilized a strain gauge load cell attached to the heave post to measure total force. The work culminates with a discussion of the fluid flow surrounding the testing specimen by particle image velocimetry experiments.

Results presented show that as a flexible plate approaches the surface, free surface effects increase the deformed plate shape when the structure is subject to regular heaving oscillations. As the plate approaches the free surface, the deformed plate shapes presented were not equivalent to those shown as the plate moved away from the free surface, suggesting free surface effects do not act uniformly on the plate at all heights. The asymmetry is further

seen in the tip deflection time histories as the plate approaches the free surface. At constant frequencies, free surface effects showed an asymptotic relationship for plate tip deflection. At a heaving frequency of 0.50 Hz, tip deflection asymptotes to 4 cm, showing that there is a critical depth that distinguishes deep water behavior from shallow water behavior.

An investigation into the effects of heaving frequency on reconfiguration showed that higher heaving frequencies retained similar trends in plate deflection over various h values. The lower two frequencies of 0.38 Hz and 0.31 Hz showed smaller deflections at the deepest h value compared to the other heights to the free surface. This suggests that lower frequencies can impact the critical point that deep water behavior occurs. By analyzing the dimensionless deflection in comparison to the height to the free surface, the asymptotic trend in plate deflection is apparent, similar to that of the constant frequency analysis. In contrast, the varied frequency experiments yielded results that asymptotes to a different dimensionless deflection for each frequency condition tested.

Strain gauge load cell experiments demonstrated that equivalent plate drag forces are experienced by the plate at the lower heaving frequency of 0.31 Hz and the higher frequency of 0.50 Hz. For both frequencies, the drag time history shifts upward as the plate moves from 30.5 cm to 6.0 cm to the free surface. The resulting time history shows higher drag forces as the plates move down, away from the free surface. The shift in drag is attributed to the asymmetry in plate reconfiguration. The fluid is able to flow at a greater rate over the plate heaving at higher frequencies, due to the increase in reconfiguration, escaping over the plate edge. Since the plate is constantly accelerating and decelerating, the lower frequency has higher added mass effects as the fluid gets trapped on top of the plate and the plate is forced to displace larger amounts of fluid throughout the oscillation.

PIV experiments, which are still very preliminary, characterized the flow field surrounding the plate edge utilizing a new dynamic masking technique that has not been seen in the

literature. Results showed that higher heaving frequencies resulted in higher flow velocities, moving from the keel to the plate edge. The flow carried over the plate edge to form a vortex before being shed as the plate transitioned its heave motion to the other direction. The lower frequency results in lower velocity for the fluid moving over the plate edge. This conclusion is consistent with the results found in the load cell experiments. As the plate is moved close to the free surface, only the upstroke forms a vortex and the fluid motion becomes asymmetric. The lack of symmetry in the fluid motion leads to the asymmetries in the plate deformations, tip kinematics, and drag discussed earlier.

4.2 Future Work

The work presented sets a strong basis for understanding the physics surrounding the problem of a flexible plate with prescribed oscillatory heaving motions close to a free surface. This thesis provides the first set of experiments in a larger project. Only one plate specimen was tested throughout the investigation. A parametric study should be carried out to investigate the effects of plate parameters such as flexural rigidity, length, and width. Such experiments will also allow for an analysis of whether or not the initial permanent set in the plate changes the measured deflections. Material properties have been identified as relevant parameters which surround the problem through Buckingham Pi theorem but were not addressed within the scope of this work. Future experiments will also include facility dependency tests. This will be completed by moving the setup and experiments to the larger tank in the Virginia Tech Hydroelasticity Laboratory, where the length of the testing section is 4.4 m.

The PIV experiments were limited to only one side of the plate, only providing insight into the fluid dynamics underneath the plate. Further experiments will be performed to characterize the fluid motion close to the free surface by completing velocity measurements

on top of the plate. Two methods may be used to complete measurements above the plate. The first would be to complete a separate set of experiments in which the laser sheet is repositioned above the tank and is aimed downward onto the plate specimen. Difficulties with this methodology include stitching the time resolved data together and matching the plate positioning at each frame. The second approach to performing PIV measurements on top of the heaving plate is to split a single laser beam into two separate laser sheets. This would allow both sides of the plate to be processed simultaneously and not require stitching of data. This method is limited by the equipment, as the laser must be strong enough such that it may be split into two laser light sheets with enough power to sufficiently illuminate the particles in the flow.

After characterizing the physics which surround an oscillating flexible plate near a free surface through image processing and PIV experiments, theoretical formulations may be established to predict the structural response to a prescribed motion or loading. This will be an important step for the progression of this work as it approaches the incorporation of flexible fluidic matrix composites (F^2MC). The F^2MCs will be incorporated into the plate design so the reconfiguration may be actively controlled to achieve desired plate shapes. The plate shape can be optimized to produce thrust on a downstroke while minimizing the drag on the upstroke, similar to a manta ray. The theoretical models established to predict the plate shape due to passive reconfiguration may then be expanded upon to include an active reconfiguration parameter. The culmination of this work will be testing in the Virginia Tech Advanced Towing Facility where an actively controlled model may be tested with forward velocity on the towing carriage.

Bibliography

[1] S. Vogel, "Drag and flexibility in sessile organisms," *Integrative and Comparative Biology*, vol. 24, pp. 37–44, 1984.

[2] S. Vogel, *Life in Moving Fluids: The Physical Biology of Flow*. Princeton, NJ: Princeton University Press, 1996.

[3] S. Vogel, "Leaves in the lowest and highest winds: Temperature, force and shape: Tansley review," *The New phytologist*, vol. 183, pp. 13–26, 05 2009.

[4] S. Alben, M. J. Shelley, and J. Zhang, "Drag reduction through self-similar bending of a flexible body," *Nature*, vol. 420, pp. 479–481, 2002.

[5] S. Alben, M. J. Shelley, and J. Zhang, "How flexibility induces streamlining in a two-dimensional flow," *Physics of Fluids*, vol. 16, pp. 1694–1713, 2004.

[6] F. P. Gosselin, E. de Langre, and B. A. Machado-Almeida, "Drag reduction of flexible plates by reconfiguration," *Journal of Fluid Mechanics*, vol. 650, pp. 319 – 341, 2010.

[7] I. Nesteruk, G. Passoni, and A. Redaelli, "Shape of aquatic animals and their swimming efficiency," *Journal of Marine Biology*, vol. 2014, pp. 1–9, 2014.

[8] D. Floryan, T. Van Buren, C. Rowley, and A. Smits, "Scaling the propulsive performance of heaving and pitching foils," *Journal of Fluid Mechanics*, vol. 822, 04 2017.

[9] G. K. Taylor, R. L. Nudds, and A. L. R. Thomas, "Flying and swimming animals cruise at a strouhal number tuned for high power efficiency," *Nature*, vol. 425, pp. 707–711, 2003.

[10] D. Floryan, T. V. Buren, and A. J. Smits, "Efficient cruising for swimming and flying animals is dictated by fluid drag," *Proceedings of the National Academy of Sciences*, vol. 115, pp. 8116 – 8118, 2018.

[11] D. Floryan and C. W. Rowley, "Clarifying the relationship between efficiency and resonance for flexible inertial swimmers," *Journal of Fluid Mechanics*, vol. 853, pp. 271 – 300, 2018.

[12] F. Fish, C. Schreiber, K. Moored, G. Liu, H. Dong, and H. Bart-Smith, "Hydrodynamic performance of aquatic flapping: Efficiency of underwater flight in the manta," *Aerospace*, vol. 3, p. 20, 07 2016.

[13] S. Alben, "Optimal flexibility of a flapping appendage in an inviscid fluid," *Journal of Fluid Mechanics*, vol. 614, pp. 355 – 380, 2008.

[14] D. Floryan and C. W. Rowley, "Distributed flexibility in inertial swimmers," *Journal of Fluid Mechanics*, vol. 888, 2020.

[15] Z. Wang, Y. Wang, J. Li, and G. Hang, "A micro biomimetic manta ray robot fish actuated by sma," *2009 IEEE International Conference on Robotics and Biomimetics (ROBIO)*, pp. 1809–1813, 2009.

[16] Z. Chen, T. I. Um, and H. Bart-Smith, "Bio-inspired robotic manta ray powered by ionic polymer–metal composite artificial muscles," *International Journal of Smart and Nano Materials*, vol. 3, pp. 296 – 308, 2012.

[17] K. Moored, P. Dewey, M. Leftwich, H. Bart-Smith, and A. Smits, "Bioinspired propulsion mechanisms based on manta ray locomotion," *Marine Technology Society Journal*, vol. 45, pp. 110–118, 07 2011.

Appendices

Appendix A

Prescribed Motion Repeatability

A.1 Repeatability of the Prescribed Oscillatory Motion

Repeated trials were completed for all experiments discussed in this work. The prescribed heaving motion was confirmed to be consistently repeatable for all heights to the free surface. Fig. A.1 shows the time history of the keel position for the repeated trials conducted at one height to the free surface for the constant frequency experiments.

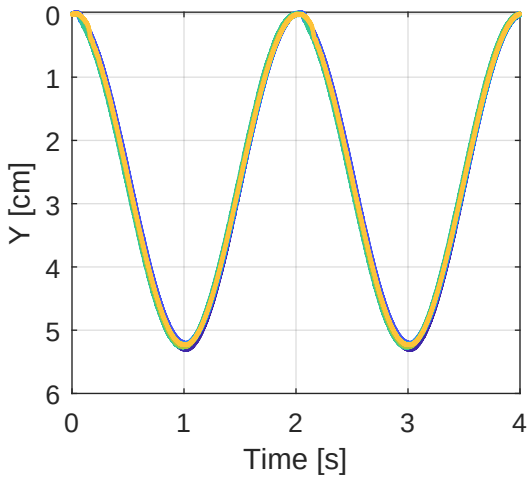

Figure A.1: Potentiometer time history agreement at one frequency and one height to the free surface.